https://ntrs.nasa.gov/search.jsp?R=19710015499 2020-03-11T20:58:10+00:00Z

General Disclaimer

One or more of the Following Statements may affect this Document

- This document has been reproduced from the best copy furnished by the organizational source. It is being released in the interest of making available as much information as possible.

- This document may contain data, which exceeds the sheet parameters. It was furnished in this condition by the organizational source and is the best copy available.

- This document may contain tone-on-tone or color graphs, charts and/or pictures, which have been reproduced in black and white.

- This document is paginated as submitted by the original source.

- Portions of this document are not fully legible due to the historical nature of some of the material. However, it is the best reproduction available from the original submission.

Produced by the NASA Center for Aerospace Information (CASI)

A UNITED STATES DEPARTMENT OF COMMERCE PUBLICATION

NBS TECHNICAL NOTE 571

Methods of Measurement for Semiconductor Materials, Process Control, and Devices

Quarterly Report

July 1 to September 30, 1970

U.S. DEPARTMENT OF COMMERCE
National Bureau of Standards

FACILITY FORM 602
N71-24975 (ACCESSION NUMBER)
(THRU)
60 (PAGES)
G3 (CODE)
CR-118271 (NASA CR OR TMX OR AD NUMBER)
26 (CATEGORY)

UNITED STATES DEPARTMENT OF COMMERCE
Maurice H. Stans, Secretary
NATIONAL BUREAU OF STANDARDS • Lewis M. Branscomb, Director

TECHNICAL NOTE 571

ISSUED APRIL 1971
Nat. Bur. Stand. (U.S.), Tech. Note 571, 58 pages (Apr. 1971)
CODEN: NBTNA

Methods of Measurement for Semiconductor Materials, Process Control, and Devices

Quarterly Report
July 1 to September 30, 1970

Edited by W. Murray Bullis

Electronic Technology Division
Institute for Applied Technology
National Bureau of Standards
Washington, D.C. 20234

Jointly Supported by the National Bureau of Standards, the Defense Atomic Support Agency, the U.S. Navy Strategic Systems Project Office, the U.S. Navy Electronic Systems Command, the Atomic Energy Commission, and the National Aeronautics and Space Administration

NBS Technical Notes are designed to supplement the Bureau's regular publications program. They provide a means for making available scientific data that are of transient or limited interest. Technical Notes may be listed or referred to in the open literature.

For sale by the Superintendent of Documents, U.S. Government Printing Office, Washington, D.C., 20402.
(Order by SD Catalog No. C 13.46:571). Price 60 cents.

PRECEDING PAGE BLANK NOT FILMED

CONTENTS

PAGE

Foreword vi

1. Introduction 1

2. Highlights 3

3. Methods of Measurement for Semiconductor Materials

3.1 Resistivity 7

3.2 Carrier Lifetime 11

3.3 Inhomogeneities 13

3.4 Gold-Doped Silicon 14

3.5 Specification of Germanium 15

3.6 References 19

4. Methods of Measurement for Semiconductor Process Control

4.1 Metallization Evaluation 21

4.2 Die Attachment Evaluation 23

4.3 Wire Bond Evaluation 23

4.4 Processing Facility 33

4.5 References 34

5. Methods of Measurement for Semiconductor Devices

5.1 Thermal Properties of Devices 35

5.2 Thermographic Measurements 42

5.3 Microwave Device Measurements 43

5.4 Carrier Transport in Junction Devices 45

5.5 Silicon Nuclear Radiation Detectors 46

5.6 References 47

Appendix A. Joint Program Staff 48

Appendix B. Committee Activities 49

Appendix C. Solid-State Technology & Fabrication Services 51

Appendix D. Joint Program Publications 52

LIST OF FIGURES

PAGE

1. Radial resistivity profiles of six *p*-type silicon wafers selected by a vendor from material now being used as commercial resistivity standards. 8

2. Infrared response spectrum of Ge(Li) Detector 619 at 77 K 16

3. A comparison of energy levels within the forbidden energy gap of germanium as determined by infrared response measurements (IRR) and by photoconductivity measurements on radiation-damaged crystals 18

4. Measured bond pull strength, T as a function of the ratio of loop height, h, to bond-to-bond spacing, d, for single level bonds 24

5. Relative positions of wire and bonding tool tip during formation of the first bond 26

6. SEM photomicrographs of typical first bonds made with various relative front-to-back motion between bonding tool and work stage 28

7. SEM photomicrographs of catastrophic failure modes that result from front-to-back motion 29

8. Electromagnetic displacement sensor mounted on an ultrasonic bonding machine to study extraneous motion between tool and work stage 30

9. Oscilloscope trace of a typical laser interferometer pattern obtained by reflecting a 0.6328-μm laser beam off the tip of a bonding tool 30

10. Ultrasonic power supply output control dial setting as a function of the vibration amplitude of the bonding tool tip 31

11. Improved electromagnetic displacement sensor 32

12. Sheet resistance of boron diffused layer in 1-Ω-cm, *n*-type silicon as a function of time 34

13. Comparison of dynamic and d-c calibration of base-emitter voltage of a 35-W, triple-diffused, silicon power transistor 36

14. Peak junction temperature of a 35-W, triple-diffused, silicon power transistor at low power levels 36

15. Comparison of peak junction temperature with average junction temperature of a 30-W, triple-diffused, silicon power transistor at low power levels 38

16. Common-emitter current gain and thermal resistance of a 35-W, triple-diffused, silicon power transistor 38

17. Junction-to-case temperature difference as derived from measurements of base-emitter voltage as a function of applied power for three different device types 39

18. Comparison of peak junction temperature with average junction temperature of a 35-W, triple-diffused, silicon power transistor 40

19. Photomicrographs of a phosphor-coated, 35-W, triple-diffused, silicon power transistor under ultraviolet illumination . . . 41

LIST OF TABLES

1. Leakage Current of a Ge(Li) Diode After Etching and Rinsing . 18

2. Threshold Adhesion Failure Loads for Aged, Highly Adherent, 0.5-μm Thick Aluminum Films on Quartz Substrates 21

FOREWORD

The Joint Program on Methods of Measurement for Semiconductor Materials, Process Control, and Devices was undertaken in 1968 to focus NBS efforts to enhance the performance, interchangeability, and reliability of discrete semiconductor devices and integrated circuits through improvements in methods of measurement for use in specifying materials and devices and in control of device fabrication processes. These improvements are intended to lead to a set of measurement methods which have been carefully evaluated for technical adequacy, which are acceptable to both users and suppliers, which can provide a common basis for the purchase specifications of government agencies, and which will lead to greater economy in government procurement. In addition, such methods will provide a basis for controlled improvements in essential device characteristics, such as uniformity of response to radiation effects.

The Program is supported by the National Bureau of Standards,[†] the Defense Atomic Support Agency,[*] the U. S. Navy Strategic Systems Project Office,[§] the U. S. Navy Electronics Systems Command,[+] the Atomic Energy Commission,[#] and the National Aeronautics and Space Administration.[×] There is not a one-to-one correspondence between the tasks described in this report and the projects by which the Program is supported. Although all sponsors subscribe to the need for the entire basic program for improvement of measurement methods for semiconductor materials, process control, and devices, the concern of certain sponsors with specific parts of the Program is reflected in planning and conduct of the work.

---

† Through Research and Technical Services Projects 4251120, 4251123, 4251126, 4252114, 4252119, 4252128, 4254111, 4254112, and 4254115.

* Through Order EA071-801. (NBS Project 4259522)

§ Administered by U. S. Naval Ammunition Depot, Crane, Indiana through Project Orders PO-1-0030 and PO-1-0041. (NBS Project 4259533)

+ Through Project Order PO-1-1057. (NBS Project 4252534)

Division of Biology and Medicine. (NBS Project 4259425)

× Through Order S-70003-G, Goddard Space Flight Center. (NBS Project 4254429)

METHODS OF MEASUREMENT FOR
SEMICONDUCTOR MATERIALS, PROCESS CONTROL, AND DEVICES

Quarterly Report
July 1 to September 30, 1970

ABSTRACT

This quarterly progress report, ninth of a series, describes NBS activities directed toward the development of methods of measurement for semiconductor materials, process control, and devices. Work is continuing on measurement of resistivity, carrier lifetime, and electrical inhomogeneities in semiconductor crystals; specification of germanium for gamma-ray detectors; evaluation of wire bonds, metallization adhesion, and die attachment; measurement of thermal properties of semiconductor devices and electrical properties of microwave devices; and characterization of silicon nuclear radiation detectors. New effort is being started on the measurement of transit-time and related carrier transport properties in junction devices. Supplementary data concerning staff, standards committee activities, technical services, and publications are included as appendixes.

Key Words: Alpha-particle detectors; aluminum wire; base transit time; carrier lifetime; die attachment; electrical properties; epitaxial silicon; gamma-ray detectors; germanium; gold-doped silicon; metallization; methods of measurement; microelectronics; microwave devices; nuclear radiation detectors; probe techniques (a-c); resistivity; semiconductor devices; semiconductor materials; semiconductor process control; silicon; thermal resistance; thermographic measurements; ultrasonic bonder; wire bonds.

1. INTRODUCTION

This is the ninth quarterly report to the sponsors of the Joint Program on Methods of Measurement for Semiconductor Materials, Process Control, and Devices. It summarizes work on a wide variety of measurement methods that are being studied at the National Bureau of Standards. Since the Program is a continuing one, the results and conclusions reported here are subject to modification and refinement.

Nearly twenty tasks, each directed toward a particular material or device property or measurement technique, have been identified as parts of the Program. The report is subdivided according to these tasks.

INTRODUCTION

Highlights of activity during the quarter are given in Section 2. Section 3 deals with tasks on methods of measurement for materials; Section 4, with those on methods of measurement for process control; and Section 5, with those on methods of measurement for devices. References for each section are listed in a separate subsection at the end of that section.

An important part of the work which generally goes beyond the task structure is participation in the activities of various technical standardizing committees. The list of personnel involved with this work given in Appendix B suggests the extent of this participation.

The report of each task includes the long-term objective, a narrative description of progress made during this reporting period, and a listing of plans for the immediate future. Additional information concerning the material reported may be obtained directly from individual staff members connected with the task as indicated throughout the report. The organization of the Joint Program staff and telephone numbers are listed in Appendix A.

Background material on the Program and individual tasks may be found in earlier reports in this series as listed in Appendix D. From time to time, publications that describe some aspect of the program in greater detail are prepared. Current publications are also listed in Appendix D.

2. HIGHLIGHTS

Highlights of the technical activity during this reporting period are presented in this section; details are given in subsequent sections of the report.

Resistivity — As part of the study of the effects of probe force and current level on the four-probe method directed toward application of the method on very thin layers, measurements have been completed on wafers with mechanically polished surfaces at 50 and 100 g probe loadings. No significant dependence on probe pressure or current level was observed. A program for reduction of the four-probe data has been written for use on the time-shared computer.

Nineteen returns have been received from the questionnaire sponsored by ASTM Committee F-1 on the need for silicon resistivity standards. While these respondees seem to have a definite interest in standard resistivity specimens, the responses are too diverse to allow immediate implementation of a course of action.

Effort continued on the identification and elimination of causes of measurement instability in the spreading resistance method. Capacitance-voltage measurements continued to be limited by lack of low-leakage diodes.

Carrier Lifetime — Work on the photoconductive decay method for bulk carrier lifetime measurements was reviewed and detailed plans were made to expedite the completion of a revision of the procedure for this method. A circuit was designed and constructed to measure carrier lifetime in epitaxial layers by the transient metal-oxide-semiconductor capacitance method. Analysis of the steady-state surface photovoltage method as applied to carrier lifetime measurements in epitaxial layers was continued. The study to relate the transient characteristics of diodes to the minority carrier lifetime was devoted to a computer analysis of the transient behavior of depletion capacitance and to investigation of junction geometry effects.

Inhomogeneities — Three ways to quantify the correlation between resistivity profiles obtained by the photovoltaic, four-probe, and two-probe methods are being evaluated. Additional resistivity profiles are being measured by the three methods for use in this study. The time required to calculate the photovoltaic resistivity profile has been reduced substantially by the introduction of computer analysis of the data.

Gold-Doped Silicon — A study of the influence of crystal quality and diffusion atmosphere on the diffusion of gold in silicon was begun. Room temperature resistivity and Hall effect measurements were completed on Hall bars cut from gold-diffused, 1-Ω-cm, *n*- and *p*-type wafers.

Specification of Germanium — Analysis of experimental data on carrier lifetime in Ge(Li) detectors carried out during the course of work on a

model for carrier trapping has yielded information on the dependence of lifetime on electric field in germanium crystals which exhibit electron trapping. The infrared response spectrum of Ge(Li) detectors has been found to have previously unobserved structure which may be due to residual levels within the forbidden energy gap of germanium. A study of the effects of certain chemical etching solutions and post-etch rinses on the diode characteristics of Ge(Li) detectors has been completed.

Metallization Evaluation — The scratch test behavior of diamond styli with nominal tip radius of about 120 μm was examined. Scratches were made in aged aluminum films, approximately 0.5 μm thick, deposited on fused quartz substrates. In some cases the test was able to discriminate between differential loads as small as 0.1 g. However, in other cases, unusual track characteristics were observed and a threshold failure load could not be established.

Die Attachment Evaluation — Improvements were made in the circuitry for measuring the thermal resistance and transient thermal response of low-power diodes. Initial measurements of thermal resistance were made on a number of diode chips which had been bonded to TO-5 headers without intentionally introducing voids.

Wire Bond Evaluation — Study of the pull test as a means for wire bond evaluation continued; an experiment to relate the measured pull strength to bond-to-bond spacing and loop height of single level bonds was completed. The relationship found between measured pull strength and the ratio of loop height to bond-to-bond spacing differed somewhat from that predicted by a simple resolution-of-forces analysis.

Experiments were completed in which relative motion between the work stage and bonding tool was introduced parallel to the wire-feed direction. Two characteristic failure modes were observed: excessive thinning or severance of the wire near the heel of the first bond and lift-off because of a weakened weld at the wire-metallization interface.

The electromagnetic displacement sensor was improved and used to seek the sources of extraneous machine motions. The laser interferometer system was placed in service and a preliminary calibration was made.

Four capacitor microphone systems were assembled and prepared for shipment to commercial lines controlled by a sponsor. Consultation with sponsors and their contractors continued.

Processing Facility — Work on the process for fabrication of *p*-channel metal-oxide-semiconductor logic devices was continued. Improvements in the process for *p*-type diffusions were made with the introduction of oxidized boron nitride slices as the source in predeposition diffusions.

HIGHLIGHTS

Photoresist Film Evaluation — Preliminary study of the evaluation of the adhesion of photoresist films by means of the scratch test was undertaken.* Diamond tips with nominal radii of 45 and 120 μm were used to scratch several samples of photoresist deposited on oxidized silicon. Each sample exhibited different failure loads and track characteristics. Differences were also observed in different portions of the same film. The significance of these differences cannot yet be evaluated with reasonable certainty; a more exhaustive investigation of the effects of film thickness and the mechanical properties of the film on the failure load is required. These preliminary tests were conducted in room temperature air; the adhesion of photoresist films in the presence of acids and water was not tested. At the present time a formal task to continue this investigation has not been established.

Thermal Properties of Devices — The dynamic procedure for calibrating base-emitter voltage as a function of device temperature was studied in detail. At low power levels junction temperature determined by the base-emitter voltage method with the use of the dynamic calibration curve was shown to agree with that determined by both infrared radiometric and thermographic phosphor techniques.

Additional study of the thermal hysteresis effect was continued. The hysteresis associated with hot spot formation was observed directly on a transistor coated with a thermographic phosphor.

Work was also initiated through EIA Committee JS-6 on Power Transistors to undertake a preliminary round robin on power transistor thermal resistance measurements.

Thermographic Measurements — It was found that light output from phosphor coatings obtained by the flotation technique was uniform both over the surface and from wafer to wafer to within about 10 percent. It was also found that phosphor luminance stabilizes within about 15 s after the phosphor reaches a given temperature within its recommended operating range. Spatial resolution of the thermographic phosphor technique was found to be limited by the resolution of the fiber-optic probe of the photometric microscope. Resolution can be improved by reducing the diameter of the probe.

Microwave Device Measurements — Design and construction of the i-f section of the X-band mixer measurement circuit was begun. A number of advantages in the measurement have been obtained by the introduction of a square wave i-f signal.

---

* R. G. Frieser, IBM Components Division, East Fishkill Facility, made the suggestion that the scratch test be applied to the study of photoresist films and kindly supplied the specimens investigated.

HIGHLIGHTS

A review of the state of accuracy in equipment for measurement of scattering-parameters of transistors was prepared for the Task Group on S-Parameter Measurement Standard of JEDEC Committee JS-9 on Low Power Transistors.

Carrier Transport in Junction Devices — This new project was undertaken in response to a technical and economic need of high priority which developed in the application of semiconductor devices for use in a radiation environment in government programs and in the development and evaluation of these devices by industry. A preliminary study was made of problems associated with measurements of charge carrier transit time in the base region of transistors and with the measurements of the frequency at which the common-emitter current gain decreases to unity. Problems both with reproducibility of these measurements and with their interpretation as predictors of transistor degradation in radiation environments were found. Near the end of the quarter laboratory work in the transit-time area began with the construction of a delay-time bridge and the specification of purchase of components for a system based on the use of a vector voltmeter.

Silicon Nuclear Radiation Detectors — The study of electron damage effects in silicon surface-barrier detectors was completed. Fabrication of silicon lithium-drifted detectors was begun in preparation for the next phase in the electron damage study. Environmental testing of surface-barrier and lithium-drifted silicon radiation detectors continued.

Standardization Activities — Program staff members are working closely with ASTM Committee F-1 as it begins to expand its activities in the process control and device evaluation areas. This expansion of activities, which is consistent with a broadened scope for the committee now being considered by the ASTM, is expected to involve first test methods for evaluation of die and wire bonds and methods for characterizing chips destined for use in hybrid microcircuits. Consideration is also being given to the development of test methods for use in determining response of electron devices to radiation environments.

This increased participation in standardization activity continues a pattern developed throughout FY-1970 Review of activity for the past three fiscal years indicates that the activity during FY-1970 was nearly equal to the total activity during the two preceding fiscal years. Over the same period, increased dissemination of program results was achieved through broader distribution of reports, more visits and visitors, and intensified direct consultation in critical areas.

3. METHODS OF MEASUREMENT FOR SEMICONDUCTOR MATERIALS

3.1 RESISTIVITY

Objective: To develop methods, suitable for use throughout the electronics industry, for measuring resistivity of bulk, epitaxial, and diffused silicon wafers.

Progress: As part of the study of the effects of probe force and current level on the four-probe method, measurements have been completed on wafers with mechanically polished surfaces at 50 and 100 g probe loadings. No significant dependence on probe pressure or current level was observed. A program for reduction of the four-probe data has been written for use on the time-shared computer. Nineteen returns have been received from the ASTM Committee F-1 questionnaire to establish the extent of the need for silicon resistivity standards. While these respondees seem to have a definite interest in standard resistivity specimens, the response was too diverse to allow immediate implementation of a course of action. Effort continued on the identification and elimination of causes of measurement instability in the spreading resistance method. Capacitance-voltage measurements continued to be limited by lack of low-leakage diodes.

Four-Probe Method — Measurements have been continued on the set of seven silicon specimens in the resistivity range 0.001 to 100 Ω-cm as part of the study of the effect of current level, probe force, and specimen surface preparation on four-probe resistivity measurements. In the present measurements, the specimens had mechanically polished surfaces and were measured at probe loadings of 50 and 100 g. The data showed less than 1 percent variation in mean measured resistivity as a function of current for nearly all specimens; no systematic variation with current was observed. This is in contrast to measurements on these specimens with lapped surfaces which showed as much as a 2 percent increase in resistivity with increasing current in the lower resistivity slices at the same probe pressures (NBS Tech. Note 555, p. 7). It was found by monitoring current supply compliance voltage that breakdown voltage was reached at the current probes for low-resistivity silicon with polished surfaces. The lack of current dependence may occur since the effect of carrier injection, which accompanies breakdown, is opposite to the effect of localized heating that had been observed previously on lapped wafers.
(J. R. Ehrstein, F. H. Brewer, and D. R. Ricks)

A program for the reduction of the four-probe data has been written for use on the time-shared computer. This program computes correction factors for specimen thickness, diameter, and temperature and allows inclusion of a correction for unequal probe spacing. In addition, it may be used in computing off-center measurements made for resistivity profiles.
(W. E. Phillips and J. P. Sinkovic)

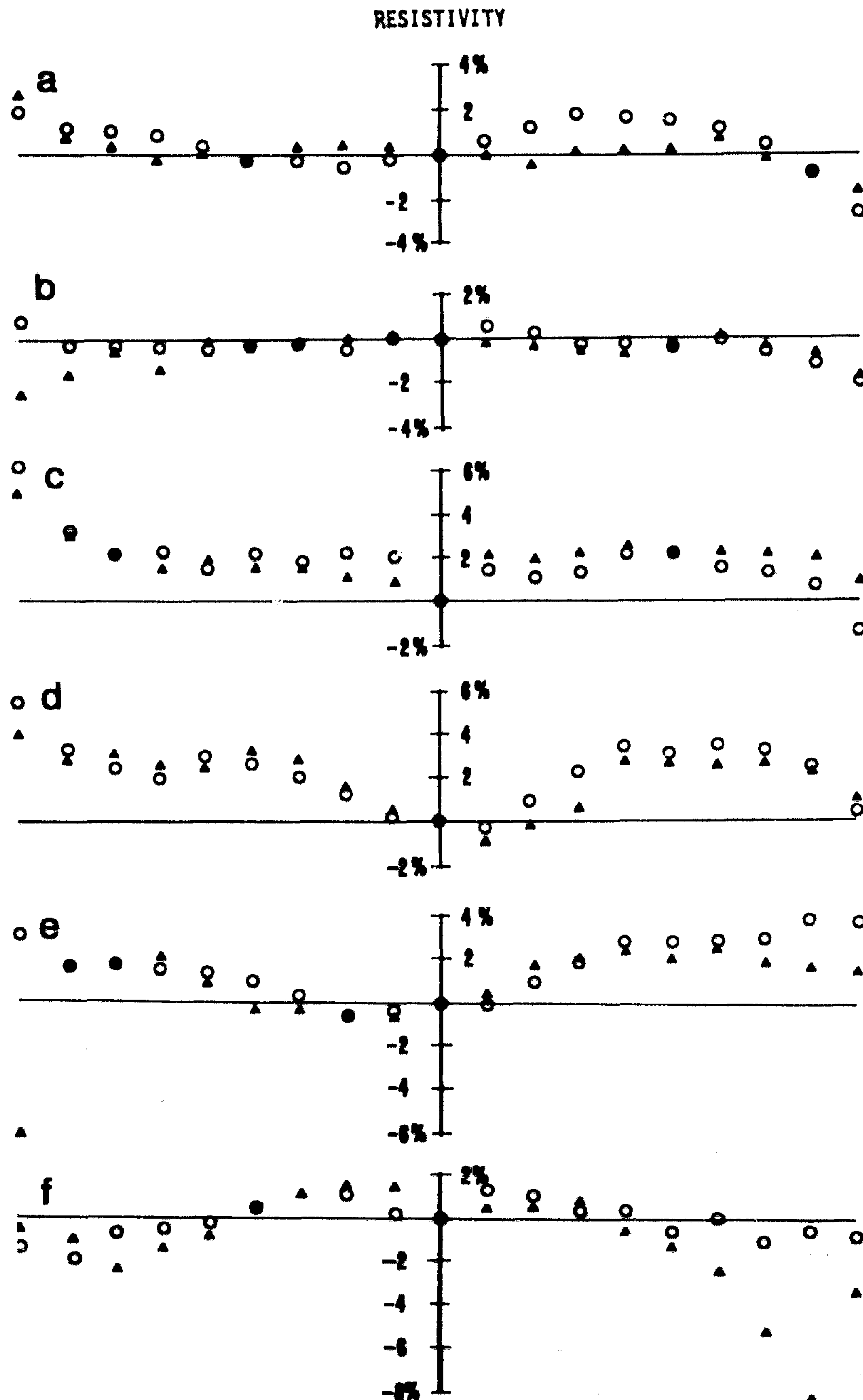

Fig. 1 Radial resistivity profiles of six *p*-type silicon wafers selected by a vendor from material now being used as commercial resistivity standards. (Measurements were made at intervals of 0.1 radius along two perpendicular diameters. Vertical scale is percent difference between resistivity at the measurement point and resistivity at the center of the wafer. Wafer diameters were 2.5 to 3.2 cm. Nominal room temperature resistivity: a, 0.0008 Ω-cm; b, 0.01 Ω-cm, c, 0.08 Ω-cm; d, 1 Ω-cm; e, 20 Ω-cm; and f, 650 Ω-cm.)

RESISTIVITY

Standardization Activities — Two silicon resistivity round robins are being conducted in conjunction with ASTM Committee F-1. Data have been received for reduction and tabulation from the five of eight participants who have completed their measurements in the round robin to measure very high resistivity silicon by the four-probe method. Two more participants have completed measurements and submitted data on the measurement by the four-probe method of the resistivity of epitaxial silicon layers deposited on opposite conductivity-type substrates. There are seven more participants in this round robin. Analysis of the data is continuing. (F. H. Brewer)

Capacitance-voltage data were taken on three test diode structures and four reference capacitors as part of a capacitance-voltage round robin being conducted by ASTM Committee F-1. (G. N. Stenbakken)

At the request of ASTM Committee F-1, a questionnaire was circulated to members of the committee. Its purpose was to gauge the qualitative and quantitative need within the semiconductor industry for silicon resistivity standards. Of some 300 mailed, 19 have been returned; these show very positive interest in obtaining silicon material and in having the measured resistivity value of such material certified by or traceable to NBS. Nevertheless, the diversity of the response is such that immediate implementation of a standard sample program is not practical. (J. R. Ehrstein)

A set of six *p*-type silicon slices, furnished by one silicon vendor as typical of material being supplied as resistivity standards, has been examined. The set covered the resistivity range 0.0008 to 650 Ω-cm. In general, the radial resistivity profiles, shown in Fig. 1, appear to be uniform enough that the slices could be used in a standard sample program by NBS. However the slight skew symmetry about the center on two of the specimens necessitated establishment of a careful multiorientation average value in order to obtain reproducible results. (J. R. Ehrstein and F. H. Brewer)

Spreading Resistance Methods — Effort on the investigation of the effect of several known interferences on spreading resistance measurements continued at a temporarily reduced level. Mechanical vibration sources were studied but vibration could not be eliminated completely. A sensitive transducer (see Section 4.3, p. 32) mounted on the probe arm of one of the probe configurations indicated vibration amplitudes of about 4-μm vertical and 2-μm lateral motion from sources such as heavy footfalls in the vicinity of the instrumentation bench. In addition a new source of contact disturbance, fluctuation in line vacuum holding the specimen to the stage, has been identified; a simple vacuum ballast tank appears to be the solution. In the investigation of causes of probe skidding, techniques are being studied to improve the quality of scanning electron microscope photomicrographs of probe contact impressions. A gold flash, 10 to 20 nm thick, has been employed to obtain relatively high quality pictures with magnification greater than 5000 X. (J. R. Ehrstein)

RESISTIVITY

Capacitance-Voltage Method — Additional capacitance-voltage measurements were made on 0.25-, 0.5-, and 1.0-mm diameter diodes in a previously diffused wafer (NBS Tech. Note 560, p. 10). Most diodes measured failed to exhibit the expected constant value of impurity density as the depth of depletion into the wafer was increased. This appeared to result from the high reverse leakage current associated with these diodes. One of the smallest diodes did reach a constant value of impurity density at depths greater than 2 μm; the resistivity calculated from the impurity density was within the range of that (±1.2 percent) determined by the four-probe method. A second set of 0.8-Ω-cm *n*-type silicon wafers was profiled for radial resistivity variations in preparation for fabrication of 1-μm deep diffused diodes with diameters from 0.12 to 1.0 mm.
(G. N. Stenbakken)

Plans: Study of the current and probe force dependence of four-probe resistivity will continue on slices with mechanically polished surfaces. The low resistivity slices will be re-examined carefully in an effort to learn more about the effects of voltage breakdown and heating at the current probes. Since higher currents tend to accelerate the deterioration of the probe and since deteriorated probes are more susceptible to voltage breakdown, this study will be conducted at currents below 300 mA. On completion of the measurements on mechanically polished surfaces, a series of measurements on chemically-mechanically polished surfaces will be begun. The possibility of vapor etching the slices will also be investigated.

Results from both four-probe resistivity round-robin experiments will be reduced and tabulated. A preliminary report on the high resistivity round robin will be prepared for the January meeting of ASTM Committee F-1.

Further consideration of silicon resistivity standards, particularly in regards to a positive course of action, awaits a more significant return on the questionnaires already mailed.

At the request of the resistivity section of ASTM Committee F-1, existing temperature-coefficient-of-resistivity data for silicon will be studied to determine whether they are suitable for converting measurements to 20°C and 25°C as alternate reference temperatures in addition to the standard reference temperature of 23°C.

Further attention will be given to the problem of obtaining spreading resistance contacts which are stable. Use will be made of the scanning electron microscope in relating probe patterns and probe skidding to measurement results.

The effects of diode leakage on measured capacitance will be studied to test whether diode Q is the significant parameter to indicate quality of capacitance-voltage measurements at a given voltage level. A computer

program developed elsewhere to correct capacitance-voltage data for deviation of the diffusion profile from a step junction will be rewritten so that it can be used at the NBS Computer facility. Diffusion procedures will be modified in efforts to obtain diodes with lower leakage current and higher breakdown voltage.

3.2 CARRIER LIFETIME

Objective: To determine the fundamental limitations on the precision and applicability of the photoconductive decay method for measuring minority carrier lifetime and to develop alternative methods for measuring minority carrier lifetime in germanium and silicon which are more precise, more convenient, or more meaningful in the specification of material for device purposes.

Progress: Much of the quarter was spent in reviewing the work on the photoconductive decay (PCD) method for bulk carrier lifetime measurements and in making detailed plans to expedite the completion of a revision of the PCD method. Work on the transient metal-oxide-semiconductor (MOS) capacitance and steady-state surface photovoltage (SPV) methods of measuring carrier lifetime in epitaxial layers continued. Study of lifetime measurements in diodes was devoted to a computer analysis of the transient behavior of depletion capacitance and investigation of junction geometry effects.

Bulk Crystals — Shortly after beginning the second set of single-laboratory, multi-operator measurements to determine the precision of the PCD method, problems were encountered with regard to signal level and specimen current selection. In its present form, the revised procedure for the PCD method specifies that the specimen current be selected based on a fixed electric field of 400 mV/cm within the specimen. With the specimen current specified in this way, photogenerated carriers sometimes drift into the end contacts. This effect, called sweep-out, results in an erroneously short lifetime measurement. Measurements were made on several specimens with the aim of establishing procedures for choosing the specimen current with the assurance that sweep-out would not be present. The interpretation of these initial measurements was obscured by specimen inhomogeneities. As a result of this difficulty detailed plans were prepared for experiments designed to resolve these problems before proceeding with the precision study. (R. L. Mattis)

Epitaxial Layers — A circuit was designed and constructed to measure carrier lifetime in epitaxial layers by the transient MOS capacitance method. The MOS capacitor is placed in a bridge with a decade capacitor. When a step voltage is applied to the bridge by switching between two independently adjustable bias levels, the MOS capacitance changes to a new value. The decade capacitor is set between the original and new

values; the time at which the transient MOS capacitance equals the decade capacitance is indicated by a null signal on an oscilloscope. Changing the decade capacitance shifts the null; the capacitance transient is constructed by determining the capacitance as a function of time after the application of the step voltage. (R. L. Mattis)

Analysis of the SPV method as applied to carrier lifetime measurements in epitaxial layers was continued. The epitaxial-substrate boundary conditions were modified to permit a photovoltage at the boundary. With this change, the analysis can be used to interpret the results of experimental measurements which could not be interpreted on the basis of the original analysis. (W. E. Phillips)

Diodes — The study relating the transient characteristics of diodes to the minority carrier lifetime concentrated on the role of capacitance and junction geometry in the transient process. The transient behavior of the depletion capacitance was analyzed by use of a computer-aided design program. The device parameters of a diode were introduced into the program and the transient behavior calculated. However, this program uses a one-lump model of the diode. Such a one-lump model does not approximate the transient response of the diode with sufficient accuracy. Therefore, this work was discontinued until a more suitable diode model can be programmed.

Commercial alloyed diodes were purchased in an attempt to obtain diodes with abrupt junctions, which would satisfy the theoretical assumptions. The lifetime in these diodes was measured by both the voltage decay and reverse recovery techniques. The previously reported discrepancy between the two techniques was again observed with these diodes. The junction geometry of these devices was then analyzed by the capacitance-voltage technique. These measurements revealed that most of the diodes did not have an abrupt junction.

By use of the data on junction geometry, an effort is being made to correlate junction geometry with the discrepancy between the two transient techniques. A group of diffused diodes is being included in this study. The space-charge capacitance is given by

$$C \propto V^{-1/n}$$

where n depends upon the steepness of the junction. In this study, the ratio of lifetime as measured by the reverse recovery technique to lifetime as measured by the voltage decay technique is plotted as a function of n to determine if a relationship is present. Lifetime measurements on all the diodes have been completed and the C-V measurements are in progress. (A. J. Baroody)

Plans: Increased emphasis will be given to the study of PCD. A series of measurements will be made to determine the appropriate relationships for selecting the specimen current and signal level. Measurements

will be made with different values of resistance in series with the specimen. Other specifications in the standard PCD procedure will be reviewed and experiments performed where it is appropriate. Work on diode recovery will be deferred until the work on PCD is completed.

The MOS measuring circuit will be tested and calibrated. A computer program for determining the lifetime from the capacitance transient will be written. Initial measurements on MOS specimens will begin.

Increased effort will be devoted to the analysis of the SPV method as applied to measurements in thin epitaxial layers.

3.3 INHOMOGENEITIES

Objective: To develop improved methods for measuring inhomogeneities responsible for reducing performance and reliability of germanium and silicon devices and, in particular, to evaluate a photovoltaic method as a means for measuring radial resistivity gradients in germanium and silicon circular wafers without contacting the flat surfaces of the wafers.

Progress: Various means of quantifying the correlation between resistivity profiles obtained by the photovoltaic, four-probe, and two-probe methods were considered. A program was written for the time-shared computer to calculate correlation coefficients based on three assumed relationships between two methods. In the most general case the relationship between the resistivity, y, as determined at a point by one method and the resistivity, x, as determined at the same point by the second, or reference, method is $y = ax + b$, where a is the slope of the line and b is the intercept. Values of both a and b can be established from the data by means of an ordinary regression analysis.

Since it is expected that the resistivity measured by any two methods should be the same, the values of a and b should be 1 and 0, respectively. In this case the relationship is $y = x$ and the degree of correlation is given by the index of determination defined previously (NBS Tech. Note 560, pp. 14-15). Because there is an arbitrary constant in the determination of resistivity by the photovoltaic method, it is necessary to have an independent measure of resistivity at one point if the relationship $y = x$ is to be used. An estimate of this can be obtained from a four-probe measurement at the center of the wafer or from a measurement of average resistivity by the van der Pauw method [1]. The accuracy of this value is frequently poor; an alternative method of analysis that employs the relationship $y = x + b$ makes the independent determination unnecessary.

Data are being analyzed according to these three relationships. Other statistical parameters, such as the slope of the line of regression

of photovoltaic resistivity against two- or four-probe resistivity, are being computed to aid in evaluating the photovoltaic technique. From these parameters one can also calculate confidence intervals for the computed correlation coefficients and errors of estimate for the computed slopes of lines of regression.

During this period photovoltaic resistivity profiles were made on eight wafers (1 to 10,000 Ω-cm) and one bar. Four-probe profiles were made on five of the wafers and two-probe profiles were made on bars cut from two of the wafers. A computer program was written to aid in reduction of the data. Use of this program has reduced by a factor of three the time required to calculate the photovoltaic resistivity profiles after the data have been obtained.

(D. L. Blackburn and F. R. Kelly)

Plans: The statistical study and preparation of the paper describing the results of this work will continue. Preliminary work on determination of the feasibility of a plasma resonance technique to measure resistivity variations in wafers of resistivity less than about 0.01 Ω-cm will begin.

3.4 GOLD-DOPED SILICON

Objective: To characterize *n*- and *p*-type silicon doped with gold and to develop a model for the energy level structure of gold-doped silicon which is suitable for use in predicting its characteristics.

Progress: To study the influence of crystal quality on the diffusion of gold in 20-Ω-cm, boron-doped silicon wafers with a high dislocation density were diffused at 850°C and 1250°C for various times. Diffusions were made in both oxygen and argon to determine if the diffusion atmosphere plays a significant role. Low dislocation density, 10-Ω-cm, boron-doped wafers, were diffused in argon at 850°C and 1250°C for various times to study the effect of diffusion atmosphere for this material; previous diffusions (NBS Tech. Note 560, p. 17) had been carried out in oxygen.

Resistivity and Hall effect measurements were made at room temperature on Hall bars cut from gold-diffused, 1-Ω-cm, *n*- and *p*-type wafers. These properties showed the expected variation with gold concentration (a large decrease in the number of free charge carriers when the gold concentration exceeds that of the shallow dopant) with the exception of several specimens for which activation analysis gave a gold concentration considerably greater than the solid solubility at the diffusion temperature. The electrical properties measured correspond to a gold concentration equal to the solid solubility, so there appear to be difficulties in the analysis procedure which may arise from nonuniform gold distribution in the wafer.

GOLD-DOPED SILICON

Spreading resistance measurements were delayed due to equipment problems. These measurements of resistivity profiles on angle-lapped bars were intended to yield an estimate of the gold concentration as a function of depth in the wafers.

(W. R. Thurber, T. F. Leedy, and W. M. Bullis)

Plans: The gold concentration of the 10- and 20-Ω-cm silicon wafers will be determined by neutron activation analysis and the results obtained for different diffusion conditions will be compared. Resistivity and Hall effect measurements will be made on Hall bars cut from some of the wafers. Spreading resistance measurements will be made on angle-lapped bars when the apparatus is functioning. Additional boron-doped wafers will be prepared for gold diffusion.

3.5 SPECIFICATION OF GERMANIUM

Objective: To measure the properties of germanium crystals and to correlate these properties with the performance of germanium gamma-ray detectors in order to develop methods for the early identification of crystals suitable for fabrication into lithium-compensated gamma-ray detectors.

Progress: Analysis of experimental data on carrier lifetime in Ge(Li) detectors carried out in the course of work on a model for carrier trapping has yielded information on the dependence of lifetime on electric field in germanium crystals which exhibit electron trapping. More detailed work on the infrared response of Ge(Li) detectors has elucidated heretofore unseen structure in the spectrum which may be due to residual levels within the forbidden energy gap of germanium.

Characterization of Germanium — In addition to an expression which gives the variation of pulse height standard deviation, σ, with charge collection efficiency, a factor relating the dependence of carrier lifetime on applied electric field was incorporated into the model for carrier trapping in Ge(Li) detectors described previously (NBS Tech. Note 560, pp. 18-19). Data were obtained from collimated gamma-ray beam measurements on Ge(Li) detectors which showed predominantly electron trapping. These data were analyzed to determine collection efficiencies of electrons and holes, separately, as a function of irradiation position (between the $n^+ - i$ and $i - p$ junctions) and the electric field, E. Values of effective carrier lifetime for electrons, τ_n, and for holes, τ_p, were calculated from these data. The analysis showed that the average slopes of curves plotted as τ_n and τ_p against E were 0.72 and 0.61 μs-cm/V, respectively. These results are not inconsistent with several published studies on the variation of carrier trap cross-section or lifetime with field [1-4]. The use of the above relationships in the trapping model gives

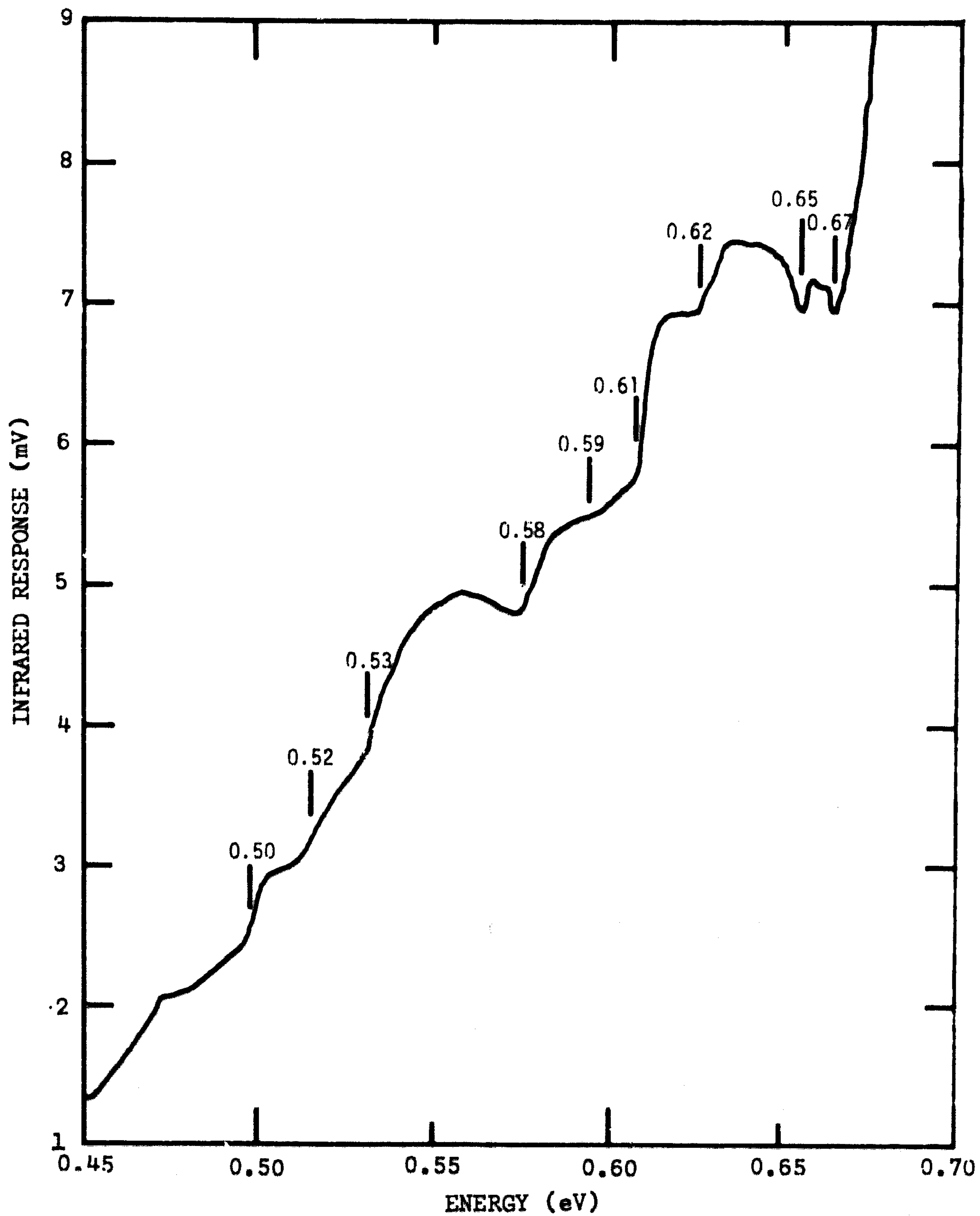

Fig. 2 Infrared response spectrum of Ge(Li) Detector 619 at 77 K.

very good agreement between experimentally observed and calculated full-energy gamma-ray peaks as a function of applied bias. The variation of σ with E accounts for the increase in tailing observed on the low-energy side of the peak, while the variation of carrier lifetime with E accounts for the observed shift of the maximum of the peak to lower energy with decreasing bias. (A. H. Sher)

Ge(Li) Detector Measurements — Work has proceeded on the evaluation of the infrared response (IRR) technique of Armantrout [5] as a possible method for measuring the quality of germanium crystals. The thickness of the germanium entrance window on the cryostat was decreased from 4 mm to 1 mm. With the thinner window the IRR spectrum shows considerably more detail than observed with the thicker window (NBS Tech. Note 555, pp. 16-19). For example, the IRR spectrum for Ge(Li) Detector 619 shown in Fig. 2 exhibits a response characteristic of discrete levels lying within the forbidden energy gap rather than the broad response previously attributed to a continuum of excited states [5].

A study was carried out using germanium entrance windows of several thicknesses ranging from 0.5 mm to 4.0 mm from several *p*- and *n*-type crystals. The IRR spectra observed were independent of the window used except for its thickness; as the thickness of the window decreased, more structure was observed in the IRR peak. Spectra obtained using a sapphire entrance window alone showed effects which can be interpreted as due to saturation of the leakage current in the detector. Short wavelength scattered radiation increases the current within the detector to such a level that the signal-to-noise ratio becomes very poor. Increases in detector leakage current by a factor of 10^4 have been observed for scattered radiation of energy greater than the bandgap energy incident on the detector through the sapphire window. The use of a germanium entrance window filters out this type of scattered radiation which is present in the monochromator.

Assuming the features indicated in Fig. 2 correspond to actual transitions into or out of a level within the bandgap, the energy level scheme shown at the left of Fig. 3 can be constructed. For comparison, defect and vacancy levels found in germanium after radiation damage measurements [6-9] are also shown. The general agreement among the energies of levels found by IRR and those seen after radiation damage is striking. The features in the IRR spectrum at 0.653 and 0.666 eV correspond to the near infrared absorption spectrum of water vapor (centered around approximately 1.9 μm) in the optical path of the monochromator system [10]. (A. H. Sher and W. J. Keery)

A study has been completed on the effects of certain chemical etching solutions and post-etch rinses on the diode characteristics of Ge(Li) diodes. Four etches and four post-etch rinses were examined. A lithium-drifted germanium diode that contained approximately 10^{15} oxygen atoms/cm^3, as determined by measurements of lithium mobility, lithium precipitation,

SPECIFICATION OF GERMANIUM

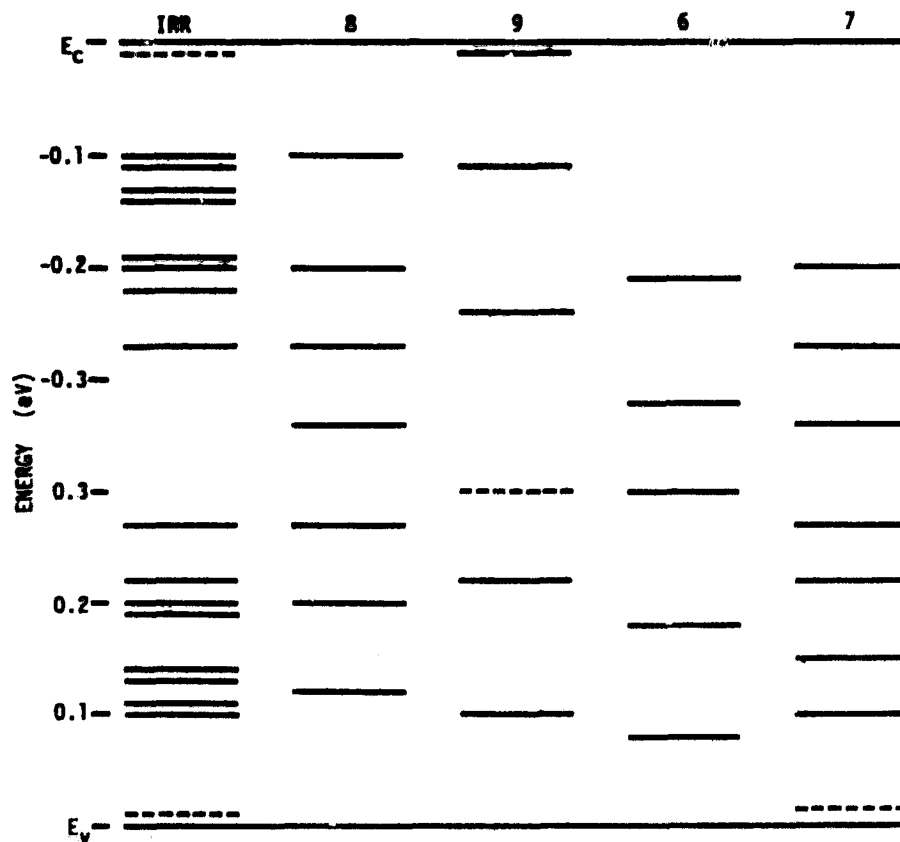

Fig. 3 A comparison of energy levels within the forbidden energy gap of germanium as determined by infrared response measurements (IRR) and by photoconductivity measurements on radiation-damaged crystals (6-9). (The number above each column corresponds to a reference cited in the text.)

Table 1 — Leakage Current of a Ge(Li) Diode After Etching and Rinsing

Rinse \ Etch	2:1:1[a]	3:1[b]	1:1[c]	CP4[d]	Rinse Averages
HF	5.0 mA	1.5 mA	1.2 mA	2.0 mA	2.4 mA
HNO_3	3.5	4.5	1.5	1.7[g]	2.8
1:3[e]	1.5	---	1.5	1.3[g]	1.4
quench/rinse[f]	1.3	2.1	1.1	1.5[g]	1.5

[a] 2 parts (by volume) 70% HNO_3, 1 part 90% HNO_3, [illegible] part 48% HF

[b] 3 parts 70% HNO_3, 1 part 48% HF

[c] 1 part 48% HF, 1 part 30% H_2O_2

[d] 30 parts 48% HF, 50 parts 70% HNO_3, 30 parts CH_3COOH, 0.5 part Br_2

[e] 1 part 48% HF, 3 parts H_2O

[f] 95% methanol quench before H_2O rinse

[g] Same value as in room air; in all other cases, leakage current in room air was greater than in nitrogen

and infrared absorption was used as the test vehicle. Since the quality of the various etches and rinses was evaluated on the basis of the measured reverse leakage current of the diode at room temperature under a nitrogen gas ambient, the oxygen-doped specimen was used so that changes in current due to room temperature diffusion of mobile lithium ions were minimized; oxygen forms an immobile donor complex with lithium ions.

The procedure used was to etch the crystal for 4 min in the etching solution after which it was rinsed in the post-etch solution in a separate beaker for 15 s. The crystal was then washed in methanol and dried with nitrogen gas. From two to seven runs were performed for each combination of etching solution and post-etch rinse. Lapping of the specimen edges between treatments was shown to have little effect on the leakage current, so in some cases the etch was performed on a previously etched surface.

The results of this study are shown in Table 1 which gives the value of leakage current of the Ge(Li) diode at 200 V reverse bias. Some variability was encountered in the leakage current measurement for several uses of the same treatment. This may be attributed, in part, to changes in the composition of the etchants with time, since it appeared that the maximum shelf-life of any of the acid mixtures was at most three weeks. On the average, the 1:3 rinse and the methanol quench/water rinse gave the lowest values of reverse current with all the etchants. Armantrout [11] studied various surface treatments for reducing the leakage current of Ge(Li) diodes at 77 K. His finding that the methanol quench treatment gives the most satisfactory results is confirmed by the present study. (E. A. Simmons and H. E. Dyson)

Plans: Study and correlation of measurements of lithium driftability, infrared response, and distribution of etch pits, three of the most promising methods for characterizing germanium for Ge(Li) detectors, will continue with the aim of developing one or more of these methods into a meaningful test for the rapid and proper specification of detector-grade germanium. Specially doped germanium crystals will be examined using the infrared response of detectors fabricated from these crystals to gain further knowledge about the results of the IRR measurements. To aid in the evaluation of these methods, measurement and interpretation of Ge(Li) detector characteristics with standard experimental methods and theoretical models will be continued.

3.6 REFERENCES

3.3 Inhomogeneities

1. L. J. van der Pauw, "A Method of Measuring Specific Resistivity and Hall Effect of Discs of Arbitrary Shape," *Philips Research Reports* 13, 1-9 (1958).

REFERENCES

3.5 Specification of Germanium

1. S. M. Koenig, R. D. Brown, and W. Schillinger, "Electrical Conduction in n-Type Germanium at Low Temperatures," *Phys. Rev.* 128, 1668-1696 (1962).

2. D. R. Hamann and A. L. McWhorter, "Cascade Capture of Electrons by Ionized Impurities," *Phys. Rev.* A134, 250-255 (1964).

3. E. E. Godik and M. I. Molchanov, "Influence of an Electric Field on the Frequency Dependence of the Generation-Recombination Noise in Boron-Doped Silicon," *Sov. Phys.-Solid State* 7, 2958-2959 (1965-66).

4. V. A. Besfamil'naya and V. V. Ostroborodova, "Influence of an Electric Field on the Recombination and Scattering of Carriers in p-Type Germanium with Deep Impurities," *Sov. Phys.-Semiconductors* 3, 110-112 (1969-70).

5. G. A. Armantrout, "Infrared Evaluation Techniques for Ge(Li) Detectors," *IEEE Trans. Nucl. Sci.* NS-17, No. 2, 16-23 (1970).

6. S. R. Novikov, E. E. Rubinova, and S. M. Ryvkin, Photoconductivity of Germanium Irradiated with Fast Neutrons," *Sov. Phys.-Solid State* 6, 690-691 (1964-65).

7. A. Gerasimov, S. M. Ryvkin, and I. D. Yaroshetskii, "Impurity Photoconductivity in Germanium Irradiated by Fast Electrons," *Sov. Phys.-Solid State* 6, 543-550 (1964-65).

8. R. F. Konopleva, et. al., "Radiation Defects in Germanium Irradiated with High Energy Protons," *Sov. Phys.-Semiconductors* 3, 948-951 (1969-70).

9. H. Y. Fan and K. Lark-Horowitz, in *Semiconductors and Phosphors*, M. Schön and H. Welker, ed. (Wiley, New York, 1958), p. 113.

10. P. F. Vornheder and W. J. Brabbs, "Moisture Determination by Near-Infrared Spectrometry," *Anal. Chem.* 42, 1454-1456 (1970).

11. G. A. Armantrout, "Ambient Storage Effects and Mounting Problems of Very Large Volume Ge LID Detectors," *IEEE Trans. Nucl. Sci.* NS-13, No. 1, 84-92 (1966).

4. METHODS OF MEASUREMENT FOR SEMICONDUCTOR PROCESS CONTROL

4.1 METALLIZATION EVALUATION

Objective: To improve methods for measuring the properties of thin metal films with initial emphasis on the adhesion of aluminum metallization deposited on various substrates.

Progress: In order to examine the scratch test behavior when using styli of larger tip radius, a number of measurements were made on several different specimens using styli with radii two to three times those of earlier experiments. All films were aluminum, approximately 0.5 μm thick, which had been vacuum evaporated onto fused quartz slides and aged for at least two weeks. Two diamond styli of ordinary phonograph needle quality with nominal tip radii of about 120 μm were used for scribing.

All measurements were carried out according to the up-and-down design; the threshold adhesion failure criterion was applied as described in earlier reports. The results of these measurements are shown in Table 2. When using a stylus with a relatively large tip radius of curvature, very adequate sensitivities are obtainable in most cases, even though

Table 2 – Threshold Adhesion Failure Loads for Aged, Highly Adherent, 0.5-μm Thick Aluminum Films on Quartz Substrates

Specimen	Stylus	Tip Radius (μm)	Increment (g)	Mean Failure Load (g)	Sample Standard Deviation (g)
L-1	D#1	113	0.1	79.04	0.25
				82.88	0.15
B3-S2	D#1	113	0.2	345.5	0.06
			0.5	341.1[a]	1.4
				348.9[a]	1.6
				343.8	0.6
B1-S3	D#1	113	1.0	424.1	1.2
				424.3	2.9
B4-S1	D#3	120	0.5	231.8	4.2
			2.0	244.4	7.2
B4-S3	D#3	120	5.0	220.4	20.7

[a] Data taken in neighboring regions of film

failure loads lie in the range of several hundreds of grams. The relatively large tip radius and failure loads notwithstanding, the scratch test can still discriminate between differential loads as small as 0.1 g. The data also reveal what appears to be a large variation in the adhesion of aluminum to quartz. This obtains despite the fact that all the samples were deposited under essentially the same conditions, and were fully aged before testing.

Although the information contained in Table 2 is illustrative of the capabilities of the scratch test for a new set of test parameters, the meaning of the data obtained was not always quite so clear. A number of hitherto unobserved "anomalies" were encountered. The track characteristics left by the styli with larger tip radius were significantly different in appearance from, or were unobserved in, tracks made by 45-μm radius styli. At loads of 200 to 300 g impressions of semicircular crescents remained within the boundaries of the scratch as if the tracking by the stylus had been momentarily interrupted. Also, for no detectable reason, one boundary of a rather smooth and symmetrical track may suddenly become ragged. One track may be smooth while the immediately following one is unaccountably ragged. In some instances a credible threshold failure load could not be established because failures would be found at stylus loads of a few grams when loads in the vicinity of one hundred grams or more were expected. At this time, the cause of these observations cannot be ascribed with confidence wholly to the characteristics of either the film or the stylus.

The two diamond styli used in these tests were examined with great care under a microscope at magnifications up to 500 X. No evidence was found of any particular surface asperity on either tip to which any of the aforementioned scratch patterns could be attributed. However, irregularities of the diamond surfaces do "machine" the aluminum films leaving a fair quantity of chips and curls on the conical surface of the stylus. It was observed that no aluminum in a plastically deformed state adhered to the working spherical tip of the stylus. This was further corroborated by SEM observations at about 200 X. These findings are contrary to those which have been reported elsewhere [1].

(J. Oroshnik and W. K. Croll)

Plans: Experiments on aluminum films evaporated on silicon dioxide thermally grown on silicon wafers will be conducted to determine the feasibility of using an infrared sensing scheme to detect adhesion failure points. Designs for a scratch test apparatus for use in systems opaque to visible light will be considered. A series of experiments on 1-μm thick aged aluminum films on quartz substrates will be designed and carried out to establish the sensitivity and reproducibility of the scratch test on thicker films. Diamond styli with nominal tip radius of 45 μm will be used for this series. Examination of stylus scratches and failure points will continue with both optical and scanning electron microscopes.

4.2 DIE ATTACHMENT EVALUATION

Objective: To evaluate methods for detecting poor die attachment in semiconductor devices with initial emphasis on the determination of the applicability of thermal measurements to this problem.

Progress: The circuit for measuring the thermal resistance and transient thermal response of low-power diodes was debugged. A sample-and-hold unit to measure the temperature-sensitive parameter of the diode under test was built; the unit has a variable delay of 2 to 10 μs with a sampling pulse width of 1.6 μs. The design, fabrication and check-out of a temperature controlled heat sink for use with unencapsulated test devices was completed.

Measurements of thermal resistance were made on a number of diode chips bonded to TO-5 headers. For these initial measurements, no voids were introduced intentionally. Two types of diode chips were used: specially processed, square, planar, diffused diodes on chips 1.27-mm square and commercial round, mesa diodes on chips 0.95-mm square. The planar diodes had a forward voltage drop range of 2 to 3 V for forward current levels of 100 to 200 mA. These devices also had surface stability problems that caused temperature dependent anomalies in the thermal resistance calibration curve. This inability to generate a usable calibration curve made precise measurements of thermal resistance impractical. The mesa diodes had a forward voltage drop ranging from 0.8 to 1.0 V for forward current levels of 100 to 300 mA. Thermal resistance measured on five of the mesa diodes at a forward current level of 300 mA ranged from 56.8 to 69.6 deg C/W, as expected from such chips bonded to TO-5 headers. It was also found that the non-thermal switching transients that occur after the termination of the heating power pulse in the thermal resistance measurement were as high as 50 μs for the mesa diodes, while it ranged from 5 to 10 μs for the planar diodes. The sample-and-hold unit was re-designed to facilitate the measurement of the slower devices. (F. F. Oettinger, R. L. Gladhill, and T. F. Leedy)

Plans: Effort in this area will be increased at the request of one of the sponsors. Initial measurements of diode transient thermal response will be undertaken. Measurements of thermal resistance will be continued. Processing of diode chips with improved surface stability will be attempted.

4.3 WIRE BOND EVALUATION

Objective: To survey and evaluate methods for characterizing wire bond systems in semiconductor devices and where necessary to improve existing methods or develop new methods in order to detect more reliably those bonds which eventually will fail.

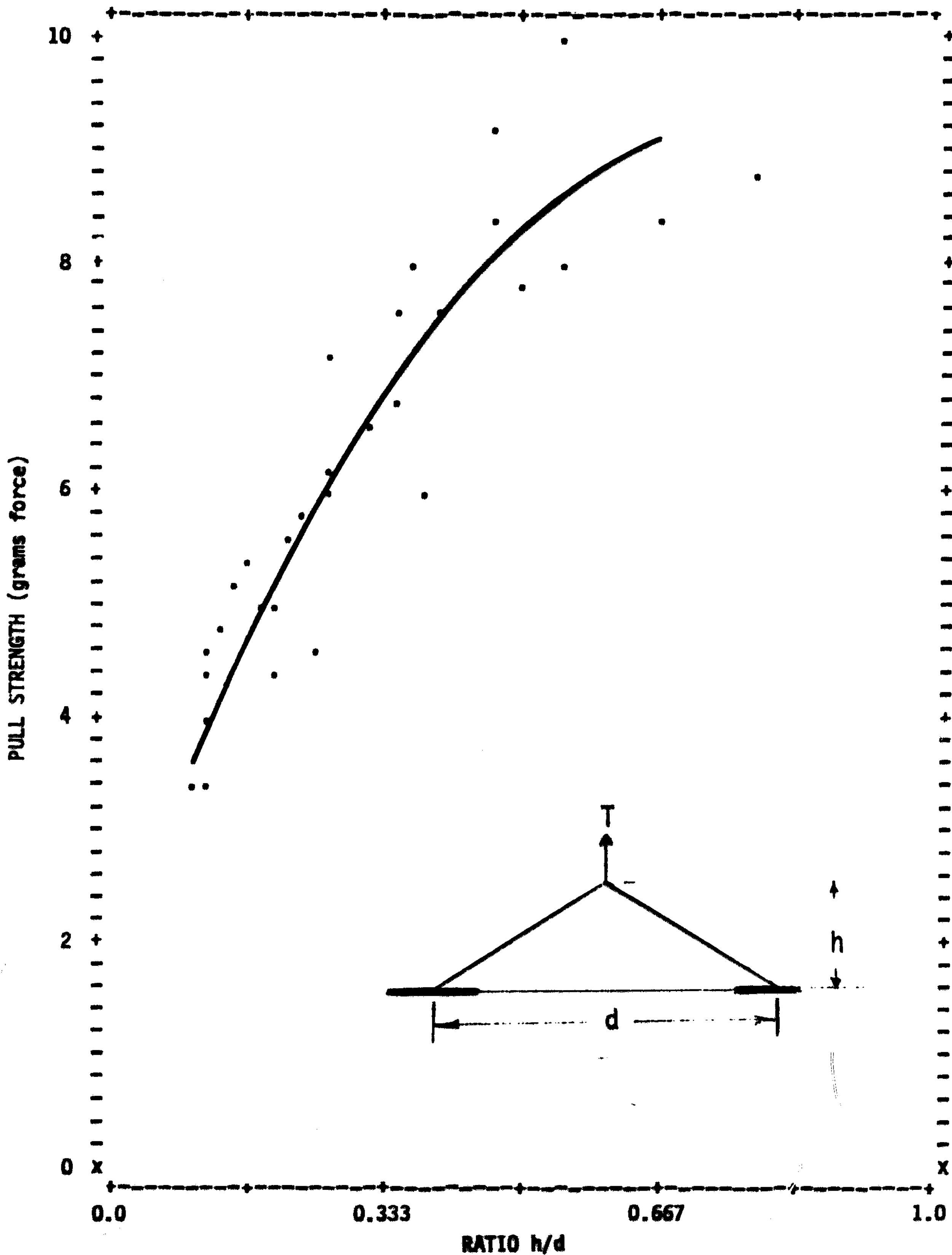

Fig. 4 Measured bond pull strength, T, as a function of the ratio of loop height, h, to bond-to-bond spacing, d, for single level bonds. (Experimental results are shown as dots. The solid line represents the equation $T = 2.0 + 19.6\,(h/d) - 13.7\,(h/d)^2$ which was the best fit over the range $0.1 < h/d < 0.6$. The geometrical quantities are shown in the inset.)

WIRE BOND EVALUATION

Progress: Study of the pull test as a means for wire bond evaluation continued; an experiment to relate the measured pull strength to bond-to-bond spacing, d, and loop height, h, of single level bonds was completed. The relationship found between measured pull strength and the ratio h/d differed somewhat from that predicted by a simple resolution-of-forces analysis.

Experiments were completed in which relative motion between the work stage and bonding tool was introduced parallel to the wire-feed direction. Two characteristic failure modes were observed: excessive thinning or severance of the wire near the heel of the first bond and lift-off because of a weakened weld at the wire metallization interface.

The electromagnetic displacement sensor was improved and used to seek the sources of extraneous machine motions. The laser interferometer system was placed in service and a preliminary calibration curve run.

Four capacitor microphone systems were assembled and prepared for shipment to commercial lines controlled by a sponsor. The level of consultation activity with sponsors and their contractors increased.

Pull Test Evaluation — Study of the pull test as a means for wire bond evaluation continued. An experiment was completed which related the measured pull strength to bond-to-bond spacing, d, and loop height, h, for single level bonds. Groups of 10 bonds each were made for 45 combinations of d and h. The value of d ranged from 1 to 2 mm and the value of h ranged from 0.12 to 1 mm. All bonds were made at the same time by a single operator in order to hold all conditions, except the variables under investigation, as nearly constant as possible. Five bonds of each group were hooked at the midpoint of the loop and pulled to destruction to determine the measured pull strength. The remaining five bonds were stressed to form the triangular shape shown in the inset of Fig. 4. From these bonds d and h were determined with a machinist's microscope. It was necessary to determine d and h on bonds other than those pulled to destruction because the effect of prestressing on the strength of the bond is not known. Except for the bonds with d = 1 mm, the spacing and loop height are operator controlled and hence subject to small variations. The mean value of d and h for each group of five were used in the subsequent analysis.

Since the measured pull strength increases as h is increased and decreases as d is increased, the mean measured pull strengths were plotted as a function of h/d as shown in Fig. 4. The data points between h/d = 0.1 and h/d = 0.6 were fitted with a quadratic also shown in Fig. 4. The quality of the fit is indicated by the fact that the residual standard deviation is 0.64 grams force (6.3 mN) which is approximately equal to the standard deviation of the pull strength around each mean value plotted. In actual practice, values of h/d greater than 0.3 would not be expected.

It should be noted that the calculated best fit is different from that predicted by a simple resolution-of-forces analysis (NBS Tech. Note 555, pp. 31-35). This difference may be due to the fact that rupture for all bonds in this experiment occurred at the crack which occurs at the heel of the first bond. This type of failure is likely to be different than an ideal fracture, such as a simple tensile break in a wire, which must be assumed if the resolution-of-forces analysis is to apply. In the present case, there is also the possibility that the nature of the heel crack varies with h or d or both. (K. O. Leedy and C. A. Main)

Characterization of Ultrasonic Bonding Systems — Experiments were continued in which relative motion between the work stage and the bonding tool was intentionally introduced in order to characterize the effects of such motion on bonding. Previously motion had been introduced transverse to the wire direction and ultrasonic tool motion (NBS Tech. Note 555, pp. 28-29, NBS Tech. Note 560, pp. 33-34). In the present study motion was introduced parallel to the wire direction and ultrasonic tool motion. As described previously, the motion was introduced by mechanically driving the work stage with an electro-mechanical transducer at various displacements and two different frequencies: 20 Hz to simulate building vibrations and 60 Hz to simulate electrical equipment vibration.

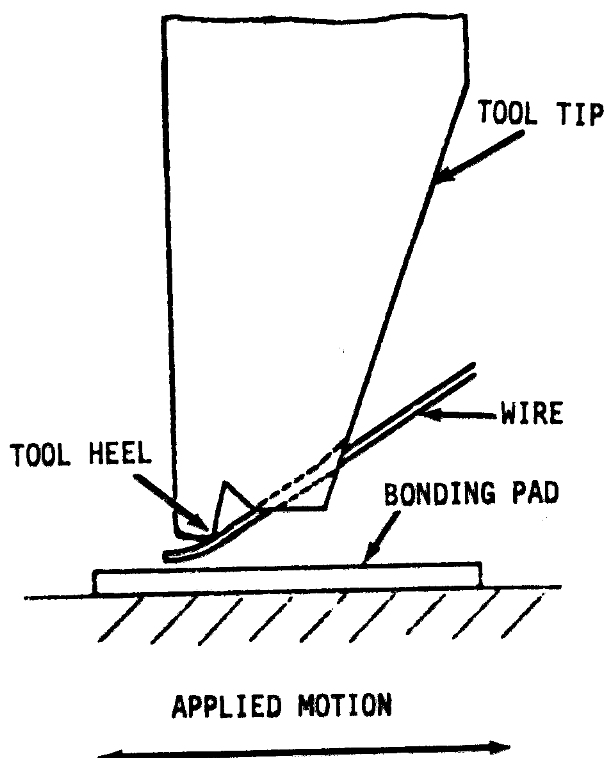

Fig. 5 Relative positions of wire and bonding tool tip during formation of the first bond.

The relative positions of the wire and tool during formation of the first bond are shown in Fig. 5. It is in this position that the normally sharp heel of the tool deforms the wire to produce the bond heel shape. The greatest effect of the front-to-back motion is on this heel shape; increased motion results in more deformation and cracking. The extent of this depends on the tool design, and, in particular, on the radius of the heel of the tool. Three tools with different heel radii were used in the test. One had a sharp heel with no intentional radius; heel radii of the others were specified as 0.2 and 0.5 mil (5 and 13 µm). Motion amplitudes of approximately 5 µm, 10 µm, and 25 µm were used at both the 20-Hz and 60-Hz driving frequencies. SEM photomicrographs of typical bonds made under these conditions are shown in Fig. 6. A bond made with the sharp-heeled tool under ordinary conditions without motion is

shown in Fig. 6a. There is only a small crack in the heel; both other tools produced similar bonds under this condition. For 5-μm motion at 20 Hz, the crack in the heel was slightly enlarged, but the actual shape of the bond was not greatly different from the case of no motion. For 10-μm motion at 20 Hz, the sharp-heeled tool almost severed the wire from the bond as shown in Fig. 6b. Increasing the motion to 25 μm often caused the wire to break. For the tool with a 13-μm heel radius less heel damage occurred. Although the heel was thinned, cracking was not severe. The deformation of the wire increased with motion, often by a factor of two in going from no motion to 25-μm motion, but the wire was not cut. An example of a bond made with the 13-μm heel radius and 25-μm motion at 20 Hz is shown in Fig. 6c.

Motion at 60 Hz produced similar results but the deformation was increased. For example, 5-μm motion at 60 Hz caused the bond to have an appearance similar to that of one made with 10-μm motion at 20 Hz. An example of a bond made with the 13-μm heel radius and 10-μm motion at 60 Hz, shown in Fig. 6d, illustrates the thinning at the heel that accompanies the increased deformation. As expected, typical bond shapes for bonds made with the tool with a 5-μm heel radius under the different motion conditions were between the two extremes just described.

Two catastrophic failure modes due to parallel motion are illustrated in Fig. 7. Actual severance of the wire due to cutting by the sharp heel is shown in Fig. 7a. Lift-off which occurs when the motion has broken the weld at the wire-metallization interface is shown in Fig. 7b. The type of failure mode depends on the portion of the bonding cycle in which the maximum motion occurs. Higher frequency motion tends to produce more reproducible and greater damage at lower displacements, since several cycles of motion may be integrated over the bonding period.
(K. O. Leedy and G. G. Harman)

The electromagnetic displacement sensor, described previously (NBS Tech. Note 560, p. 37) and improved this quarter (see p. 32), was used to seek the source of the extraneous motions which have been observed in bonding machines (NBS Tech. Note 527, p. 39; NBS Tech. Note 555, p. 29). In this application of the sensor the tape recorder head is mounted on the machine housing and the magnetic pickup is clamped to the work stage as shown in Fig. 8.

The most severe motions were found in the side-to-side and vertical directions. In the side-to-side direction, the upper part moved in relation to the work stage while going through the first and second bond cycles. A support bracket was made and mounted between upper and lower bonder parts to decrease the movement. In addition to the movement, a vibration, which results principally from the starting torque of the stepping motor and camshaft assembly, is observed. In the vertical direction, no movement such as that observed in the side-to-side direction is seen; vibration does occur but at a higher frequency. (H. K. Kessler)

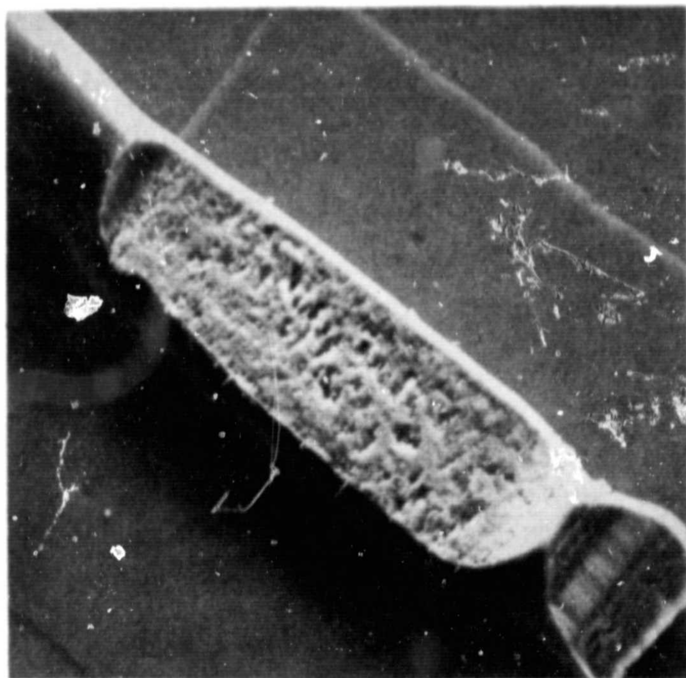

a: No motion; Magnification 235 x.

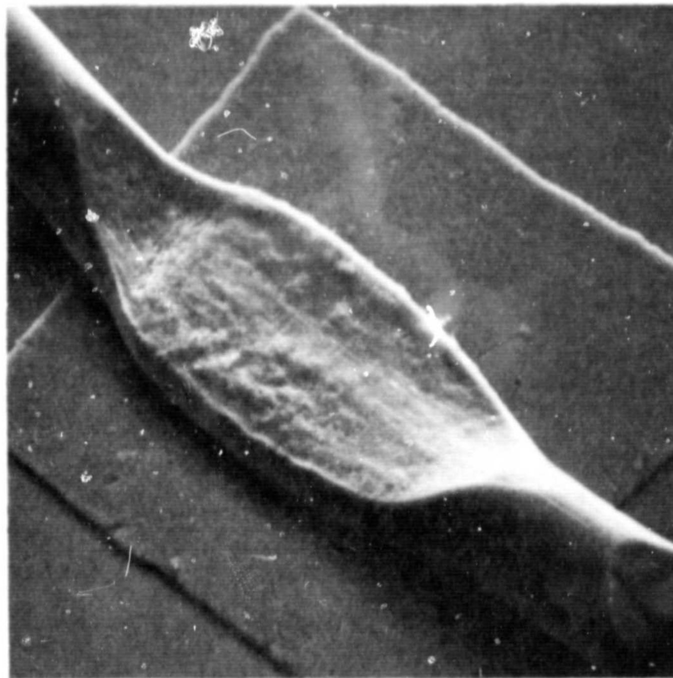

c: Amplitude: ~ 25 μm; Frequency: 20 Hz; Magnification: 500 x.

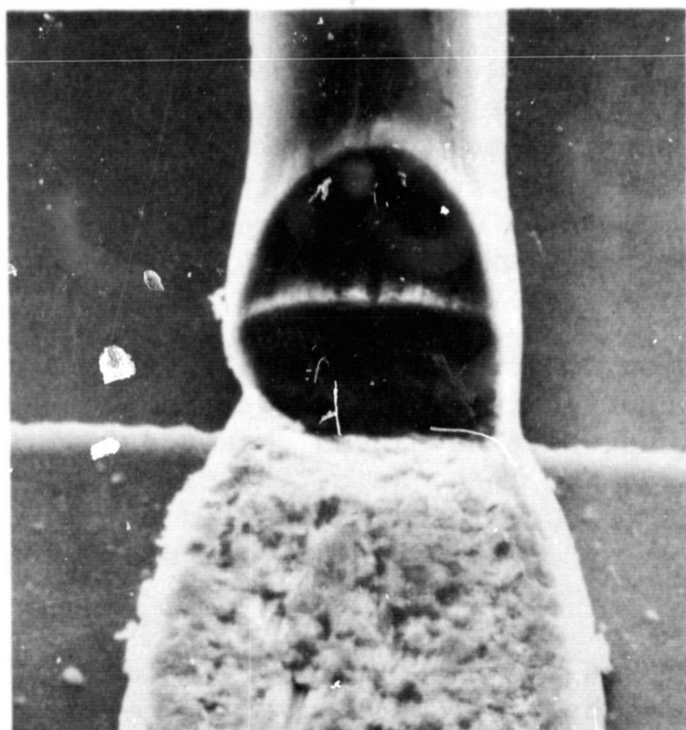

b: Amplitude: ~ 10 μm; Frequency: 20 Hz; Magnification: 500 x.

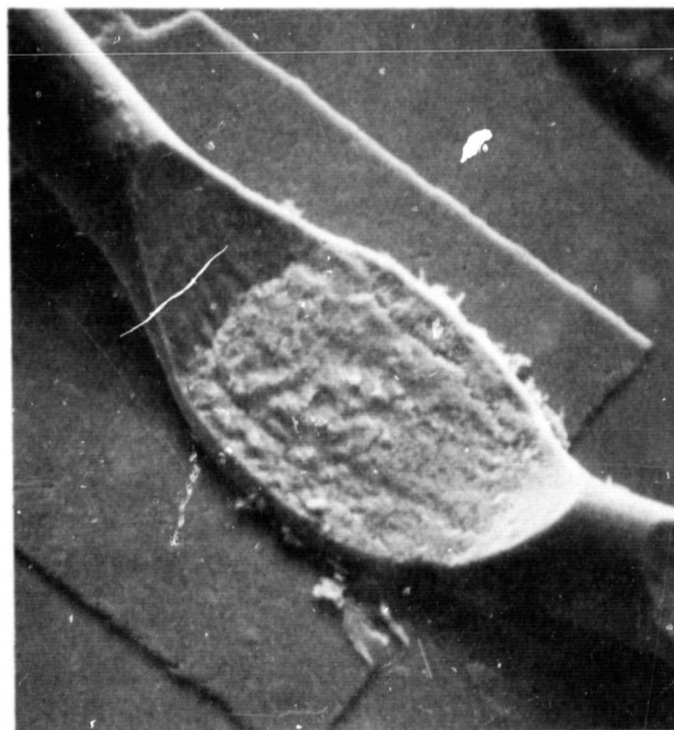

d: Amplitude: ~ 10 μm; Frequency: 60 Hz; Magnification: 480 x.

Fig. 6 SEM photomicrographs of typical first bonds made with various relative front-to-back motion between bonding tool and work stage.

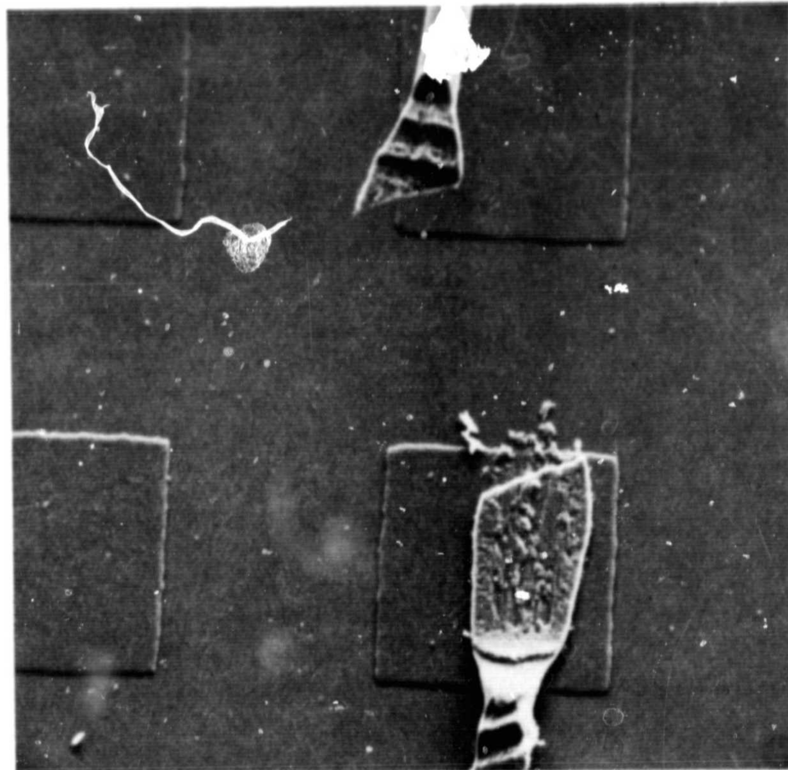

a. Severance of wire by heel of tool. Magnification: 200 x.

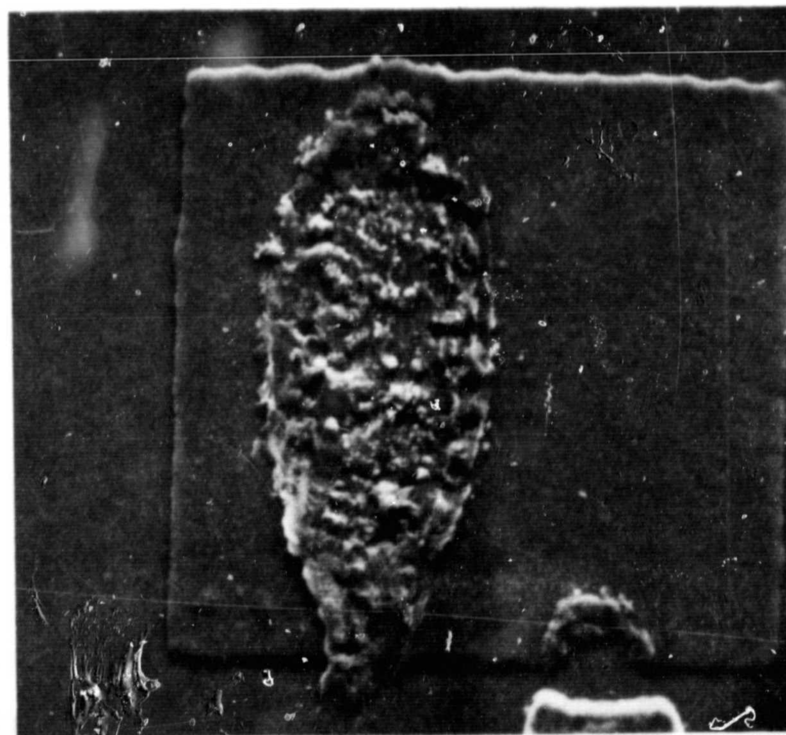

b. Lift-off at weakened weld. Magnification: 500 x.

Fig. 7 SEM photomicrographs of catastrophic failure modes that result from front-to-back motion.

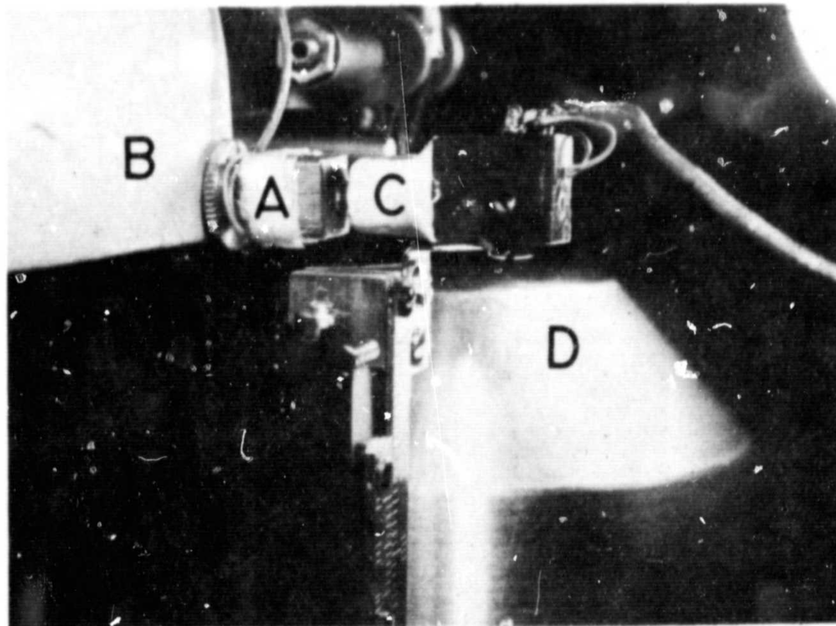

Fig. 8 Electromagnetic displacement sensor mounted on an ultrasonic bonding machine to study extraneous motion between tool and work stage.
A — Tape recorder head.
B — Machine housing.
C — Magnetic pickup coil.
D — Work stage

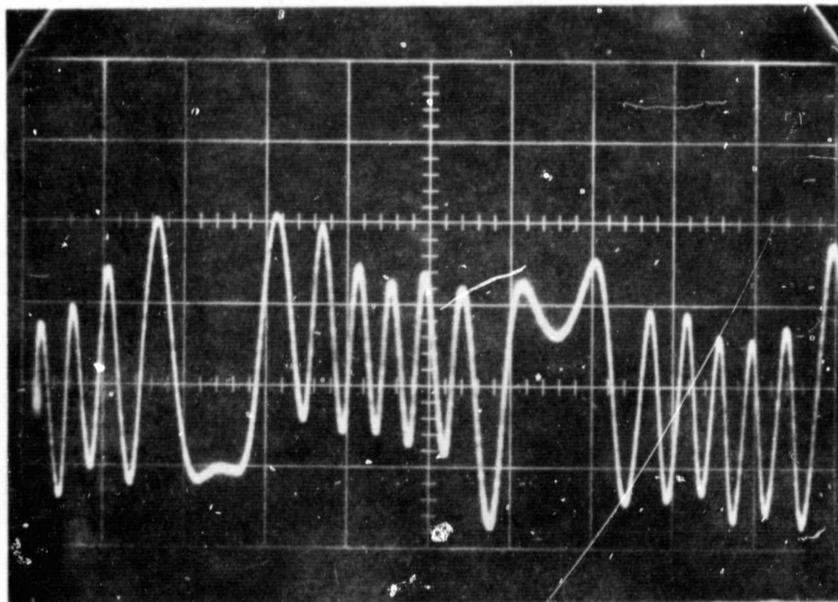

Fig. 9 Oscilloscope trace of a typical laser interferometer pattern obtained by reflecting a 0.6328-μm laser beam off the tip of a bonding tool. (The 6.6 fringes between the end points represent a vibration amplitude of 2.1 μm (82 μin.).)

The laser interferometer system previously described (NBS Tech. Note 555, p. 30) was put into use toward the end of the quarter. This system is based on a principal described by Clunie and Rock [1]; specific details and techniques have been described by Martin [2]. Utilization of the system was delayed because of the excessive amount of electrical noise generated in the laser discharge tube. This noise was reduced to an acceptable level and absolute measurements of bonding tool motion have begun. The helium-neon laser operates at a wavelength of 0.6328 μm; thus each complete interference fringe is equivalent to a bonding tool displacement of 0.316 μm. A typical interferometer pattern obtained by reflecting the laser beam off a bonding tool is shown in Fig. 9. The picture was made by photographing a single sweep of the oscilloscope beam. Approximately 6.6 fringes appear between the turn-around or end points of the motion. This represents a total displacement of 2.1 μm. The unstable base line in the figure results from low frequency noise in the system. The interferometer system was used to generate the calibration curve of ultrasonic power supply output control dial setting as a function of 59 kHz bonding tool motion shown in Fig. 10. Amplitudes between 1.3 and 2 μm (50 and 80 μin.) peak-to-peak are typically used for making single level bonds in the present studies. (G. G. Harman)

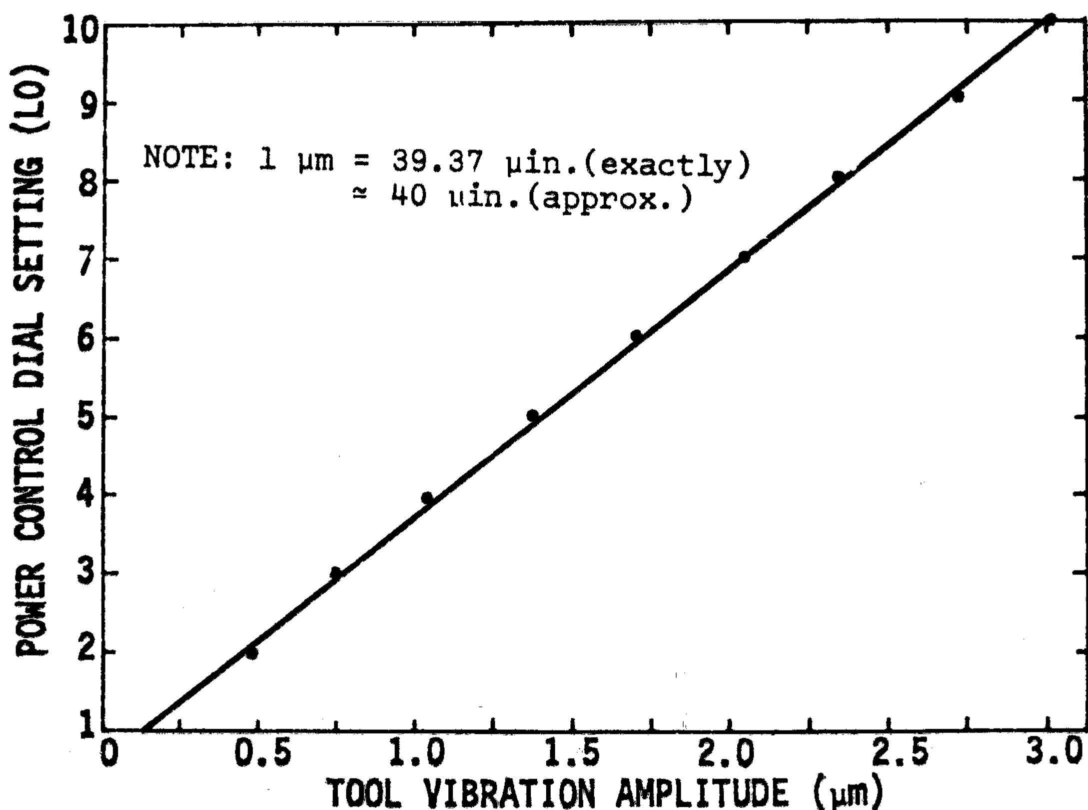

Fig. 10 Ultrasonic power supply output control dial setting as a function of the vibration amplitude of the bonding tool tip. (The driving frequency is 59 kHz; the control is set to the LO position.)

WIRE BOND EVALUATION

Four complete microphone systems were assembled and prepared for shipment to commercial lines controlled by a sponsor. The work consisted of installing high-pass, audio-rejection filters in the microphone power supplies, fabricating and installing microphone tapers, and calibrating the assembled systems with the laser interferometer. (G. G. Harman)

Equipment Improvements — The maximum sensitivity of the previously described electromagnetic displacement sensor (NBS Tech. Note 560, p. 37) was increased to 720 mV for a displacement of 25 μm. The resolution was improved and is now about 0.01 μm. The response of the sensor is linear over the measured range from 0 to 0.353 mm. Since the sensitivity is a factor of 30 higher for displacement in one direction than for displacement in the other two directions, displacements or vibrations can be separated into x, y, and z components.

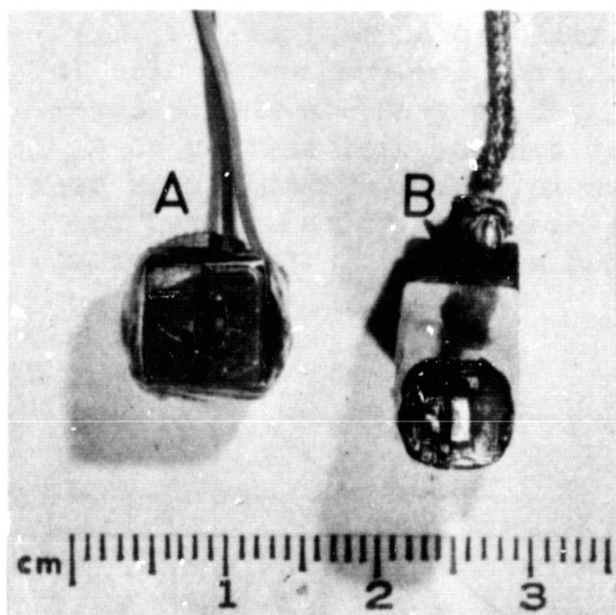

Fig. 11 Improved electromagnetic displacement sensor.
A — Tape recorder head.
B — Magnetic pickup coil.

The sensor consists of a modified tape recorder head with the gap opened up to 1.37 mm and a pickup coil with a ferrous core as shown in Fig. 11. The recorder head is driven electrically with a sine wave at approximately 100 kHz, the resonant frequency of the pickup coil. The coil is separated from the recorder head by 50 μm or more depending upon the required sensitivity. The output of the coil is displayed on an oscilloscope. (H. K. Kessler)

Bibliography and Critical Review — The first draft of the critical review survey paper was completed and work on the bibliography was continued. (H. A. Schafft and E. C. Cohen)

Plans: Experimental and statistical analysis of significant factors in the bond pull test will continue. Laser interferometer calibration and study of bonding tool motion will continue. Statistical studies for optimizing bonding parameters for two-level bonds will be undertaken. Evaluation of ribbon wire for ultrasonic bonding will resume. Work on the wire tester will continue. Further assistance will be given to sponsors in connection with problems encountered on production lines. Preparation of the final draft of the critical review survey paper will begin and work on the first draft of the bibliography will continue.

4.4 PROCESSING FACILITY

Objective: To establish a microelectronic fabrication laboratory with the facilities and procedures necessary for the production of specialized silicon devices for use in research on measurement methods.

Progress: Work on the process for fabricating p-channel metal-oxide-semiconductor (MOS) logic devices was continued. In addition to the previously reported test chip designed to facilitate the measurement of the electrical characteristics of the devices such as threshold voltage and propagation time (NBS Tech. Note 560, p. 38), a serial file register designed to implement a specific logic function was fabricated. During the production of the serial file register, the thresholds, which previously had been 3 to 4 V, became excessive. A preliminary investigation of the problem disclosed that the starting material for the faulty devices had been different than that used previously. Both device types were fabricated on <111>-orientation, (1.0 ± 0.5)-Ω-cm, n-type silicon. However, the silicon for the first devices was doped with phosphorus whereas the silicon for the second was suspected to be doped with antimony. Upon returning to phosphorus-doped material, thresholds in the 3 to 4 V range were again attained.

During fabrication of these devices, it became apparent that use of a gaseous (diborane) source for the p-type diffusion resulted in excessively large variation of the sheet resistance across the slice. The problem was corrected by changing the diffusion source to oxidized boron nitride slices [1]. Use of this source offers many advantages including the elimination of flow-pattern problems, the use of a single inert carrier gas, and compatibility with existing equipment. In use, boron nitride slices that have been thermally oxidized to convert their surfaces to boron trioxide are placed in the diffusion furnace in a boat alternately with the silicon wafers to be diffused. In this manner, each silicon slice is provided with its own large-area dopant source. Since the amount of boron is limited, the problem of sticky furnace tubes due to the reaction of excess boron with the quartz is eliminated. All predeposition diffusions for the MOS devices were done at 950 ± 1°C. A nitrogen flow of 2.5 ℓ/min was maintained in the furnace at all times. The sheet resistance of the predeposited layer obtained as a function of predeposition time is shown in Fig. 12. The variation in the sheet resistance, both after predeposition and after redistribution at 1150°C, was less than ±3 percent across a slice. Slice-to-slice variations were within ±7 percent. (T. F. Leedy and J. Krawczyk)

Plans: Work will be started on development of a method to characterize the dynamics of photoresist spinners. This is an important measurement in the control of the photolithographic process since the thickness of the photoresist film on the wafer is determined by the initial accelerations and final rotational speed of the spinner. A system will be constructed for the deposition of vitreous silicon dioxide from silane. This should prove useful as a method of masking and protecting silicon

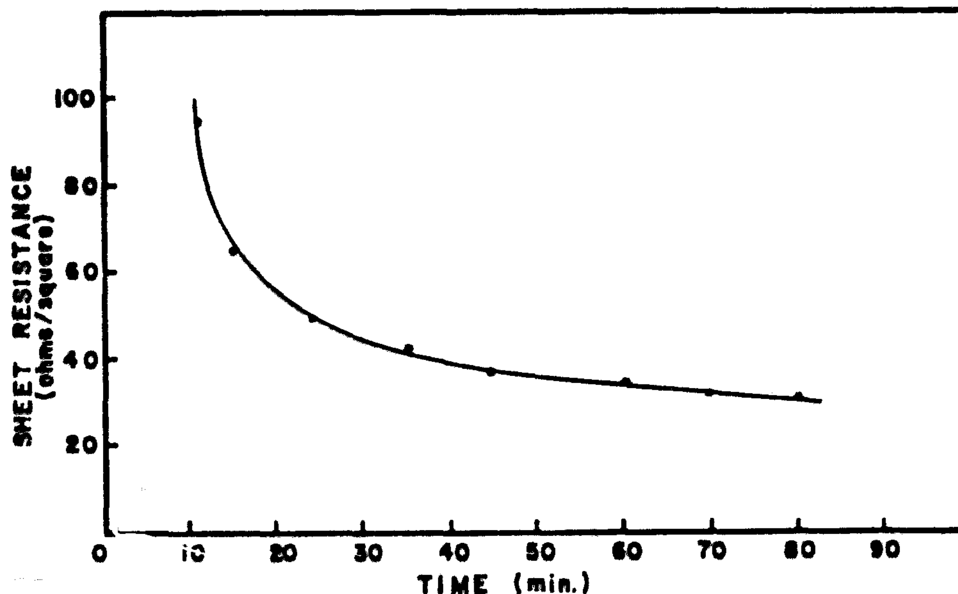

Fig. 12 Sheet resistance of boron diffused layer in 1-Ω-cm, *n*-type silicon as a function of time. (Oxidized boron nitride slices were used as the source of the boron; diffusion temperature was 950°C.)

surfaces. An electron beam evaporation system will be installed to improve the quality of aluminum metallization. Because the aluminum deposited by this system does not contain as many impurities as evaporated aluminum, it is expected that surface stability of devices will be improved after this system is placed in service.

4.5 REFERENCES

4.1 Metallization

1. D. W. Butler, C. T. H. Stoddart, and P. R. Stuart, "The Stylus or Scratch Method for Thin Film Adhesion Measurement: Some Observations and Comments," *Brit. J. Phys. D: Appl. Phys.* 3, 877-883 (1970).

4.3 Wire Bond Evaluation

1. D. M. Clunie and N. H. Rock, Jr., "The Laser Feedback Interferometer," *J. Sci. Instrum.* 41, 489-492 (1964).

2. B. D. Martin, presented at New York State Technical Services Symposium on Lasers and Their Application in Local Industries, Binghampton, N.Y., April 14, 1969.

4.4 Processing Facility

1. N. Goldsmith, J. Olmstead, and J. Scott, "Boron Nitride as a Diffusion Source for Silicon," *RCA Review* 28, 344-350 (1967).

5. METHODS OF MEASUREMENT FOR SEMICONDUCTOR DEVICES

5.1 THERMAL PROPERTIES OF DEVICES

Objective: To evaluate and, if necessary, improve electrical measurement techniques for determining the thermal characteristics of semiconductor devices.

Progress: The literature search for methods to measure thermal resistance and transient thermal response of semiconductor devices was continued. Work on the bibliography and review paper was further delayed due to work in other priority areas.

(M. Sigman and F. F. Oettinger)

Need for dynamic calibration of the temperature sensitive parameter used to measure thermal resistance, R_Θ, of a transistor has been noted previously (NBS Tech. Note 560, p. 40). In the usual case, the temperature sensitive parameter, such as the base-emitter voltage, V_{BE}, is measured as a function of device temperature. When the calibration is made under dynamic conditions, in which the transistor is switched from a very low level power-on condition to the calibration mode, a slightly different calibration curve is obtained. The differences are attributed to interferences by electrical switching transients which are more significant at low power levels. Typical static, or d-c, and dynamic calibration curves are illustrated in Fig. 13. Use of the static calibration may yield erroneous values of junction temperature which result in an apparent increase in R_Θ at low power levels. At very low power dissipation the temperature difference between case and junction should approach zero. However, the base-emitter voltage obtained for a junction temperature of 25°C obtained under dynamic test conditions is equivalent to 31°C on the d-c calibration curve. Hence use of the d-c calibration curve in this example would indicate a temperature difference of 6°C with zero power dissipation. This unrealistically implies an infinite R_Θ for this condition.

Junction temperature was determined at low power levels on a number of devices by both the infrared radiometric and thermographic phosphor techniques. A typical curve, shown in Fig. 14, reveals reasonably good agreement between the two techniques. No evidence of an increase in thermal resistance as power level is decreased is noted. Junction temperature was also determined from measurements of V_{BE} at low power levels. As illustrated in Fig. 15, good agreement is obtained between these measurements and infrared radiometric measurements when the dynamic calibration curve is used to convert V_{BE} to junction temperature.

Further tests were conducted to determine the optimum base drive for the thermal resistance measurements. Attempts to reduce the magnitude of the switching transient associated with the termination of the power pulse during the R_Θ measurement for a particular transistor type so as to

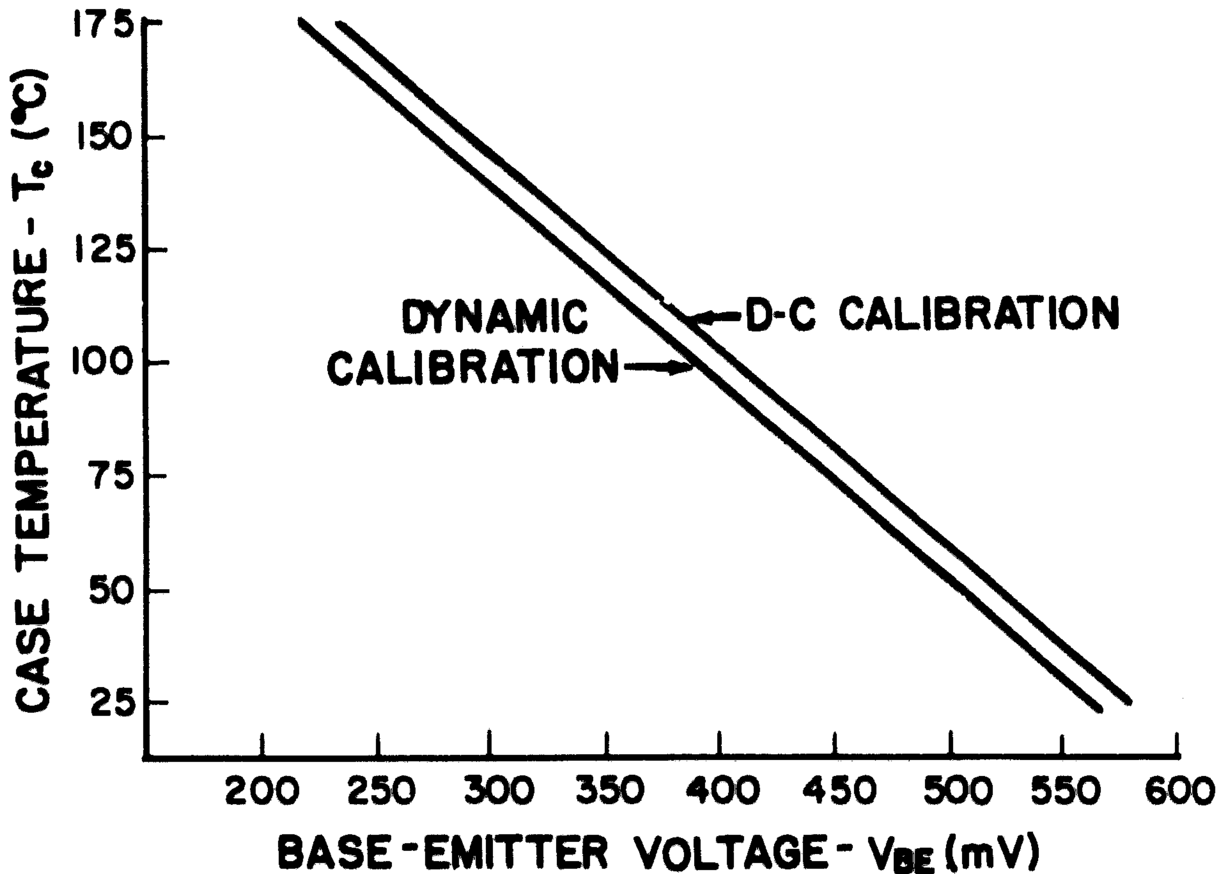

Fig. 13 Comparison of dynamic and d-c calibration of base-emitter voltage of a 35-W, triple-diffused, silicon power transistor. (In the dynamic calibration procedure the transistor under test was switched from an operating condition of V_{CE} = 1 V and I_C = 100 mA to the test condition. In both procedures the base current was controlled at 2.5 mA during measurement of base-emitter voltage.)

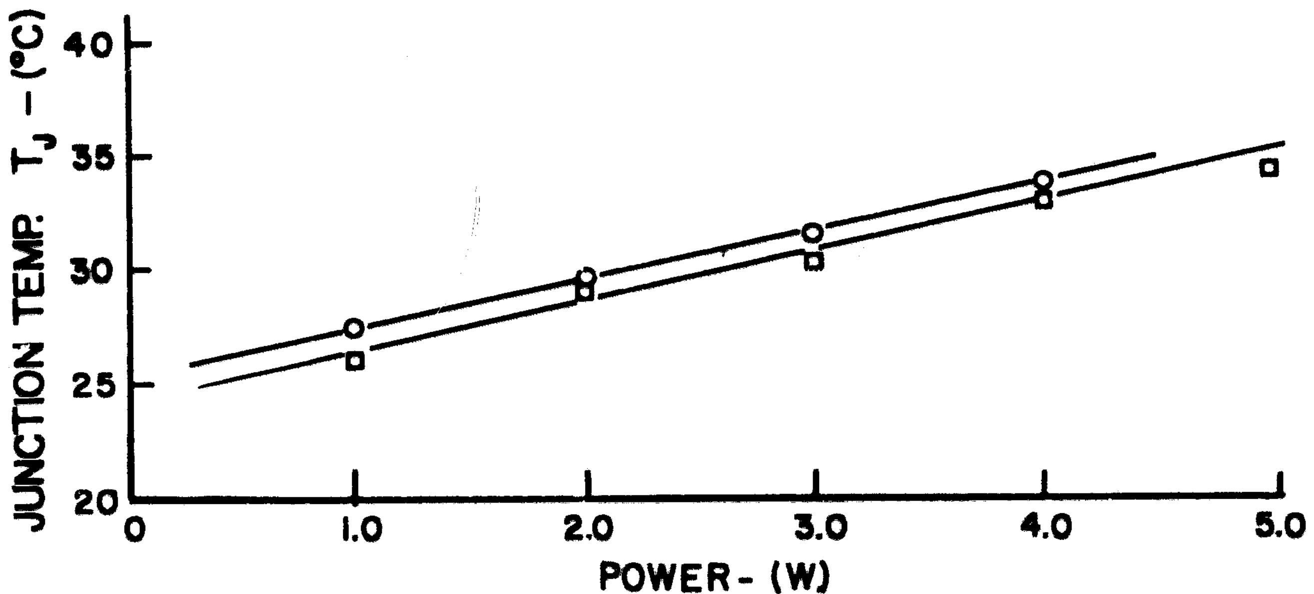

Fig. 14 Peak junction temperature of a 35-W, triple-diffused, silicon power transistor at low power levels. (Measurements were made with an infrared microradiometer (□) and thermographic phosphors (○). During the application of power, collector current was 1 A; case temperature was held at 25°C. Under low power conditions no hot spot is observed.)

negate the need for dynamic calibration were unsuccessful. It has become apparent that the optimum base drive conditions are dependent on the device construction as well as the device operating conditions.

Study of the thermal hysteresis effect observed previously (NBS Tech. Note 520, pp. 49-52) was continued. Base current, I_B, and V_{BE} were measured for constant collector current as a function of collector-emitter voltage, V_{CE}. A typical plot of common emitter current gain, h_{FE}, the reciprocal of I_B, and R_Θ, found from V_{BE} with the use of a dynamic calibration curve, as a function of applied power with constant collector current (150 mA) is shown in Fig. 16. The notable thing about both of these curves is that the voltage at which the device drops out of hysteresis is the same for both the h_{FE} measurement, in which the collector circuit is not opened, and the thermal resistance measurement, in which (in the case illustrated) the collector is opened for 20 μs. Thus it would appear that the thermal inertia of the hot spot is such as to maintain the hysteresis condition for a period significantly longer than 20 μs.

Measurements of junction temperature were made on six transistors representing three manufacturers and both triple- and epitaxial-diffused construction. Data were taken at collector current levels of 100 and 200 mA. Junction-to-case temperature difference is shown in Fig. 17 for three of the six transistors. The data indicate that, for the low collector currents used, not only is R_Θ nearly constant until hot-spot formation is initiated but that it is also the same for both current levels.

On several transistors R_Θ as determined by the V_{BE} technique was compared with the actual peak temperature on the chip surface as measured by temperature sensitive phosphors and an infrared microradiometer. An example of these measurements is illustrated in Fig. 18. Junction temperature as found from V_{BE} and infrared measurements is plotted as a function of power. As in Fig. 15 the temperatures are essentially identical at power levels below 4 W. As the power increases and the temperature and current distributions in the transistor becomes less uniform, the temperature indicated by the infrared microradiometer becomes increasingly higher than that indicated by V_{BE}. On the formation of a hot-spot at slightly over 20 W, the difference is almost three to one. At 20 W, the thermal resistance computed from the infrared measurements is almost twice as great as the value obtained from the V_{BE} measurements. It should be noted that the infrared microscope is always centered over the hottest spot on the transistor surface, while the V_{BE} measurement is, by its very nature, an integrating process. This points out the difficulty of determining the maximum junction temperature under high-voltage, high-power operating conditions with electrical techniques.

(S. Rubin and F. F. Oettinger

Hot-spot formation and the thermal hysteresis effect were also studied with thermographic phosphors. Photomicrographs of a phosphor-coated and illuminated transistor chip are shown in Fig. 19. On the left of the

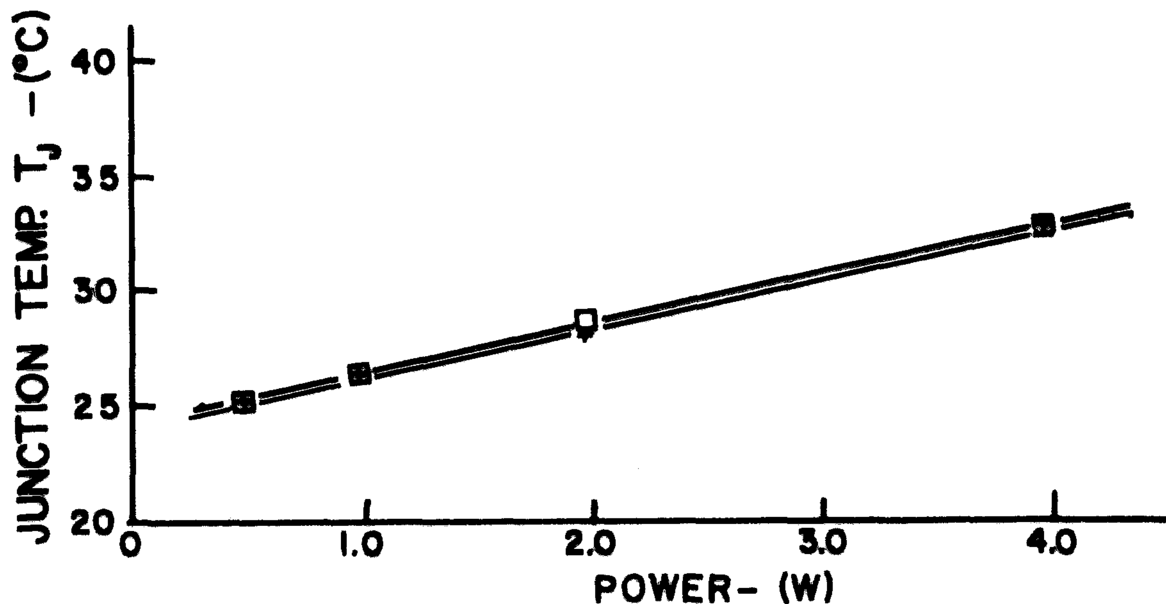

Fig. 15 Comparison of peak junction temperature with average junction temperature of a 30-W, triple-diffused, silicon power transistor at low power levels. (Peak temperature measurements were made with an infrared microradiometer (□) and average temperature measurements, by the base-emitter voltage method (+) with dynamic calibration. During application of power, collector current was 200 mA; case temperature was held at 25°C. Under low power conditions a hot spot does not form and peak and average temperatures are the same.)

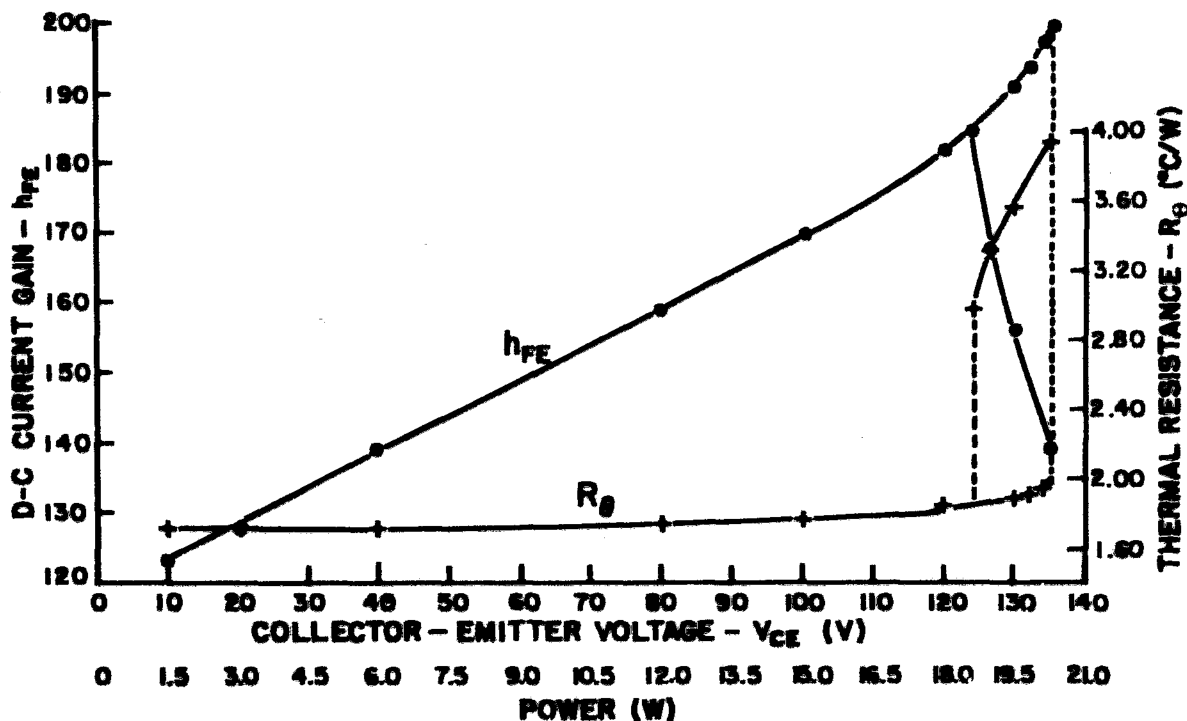

Fig. 16 Common-emitter current gain and thermal resistance of a 35-W, triple-diffused, silicon power transistor. (Case temperature was held at 25°C.)

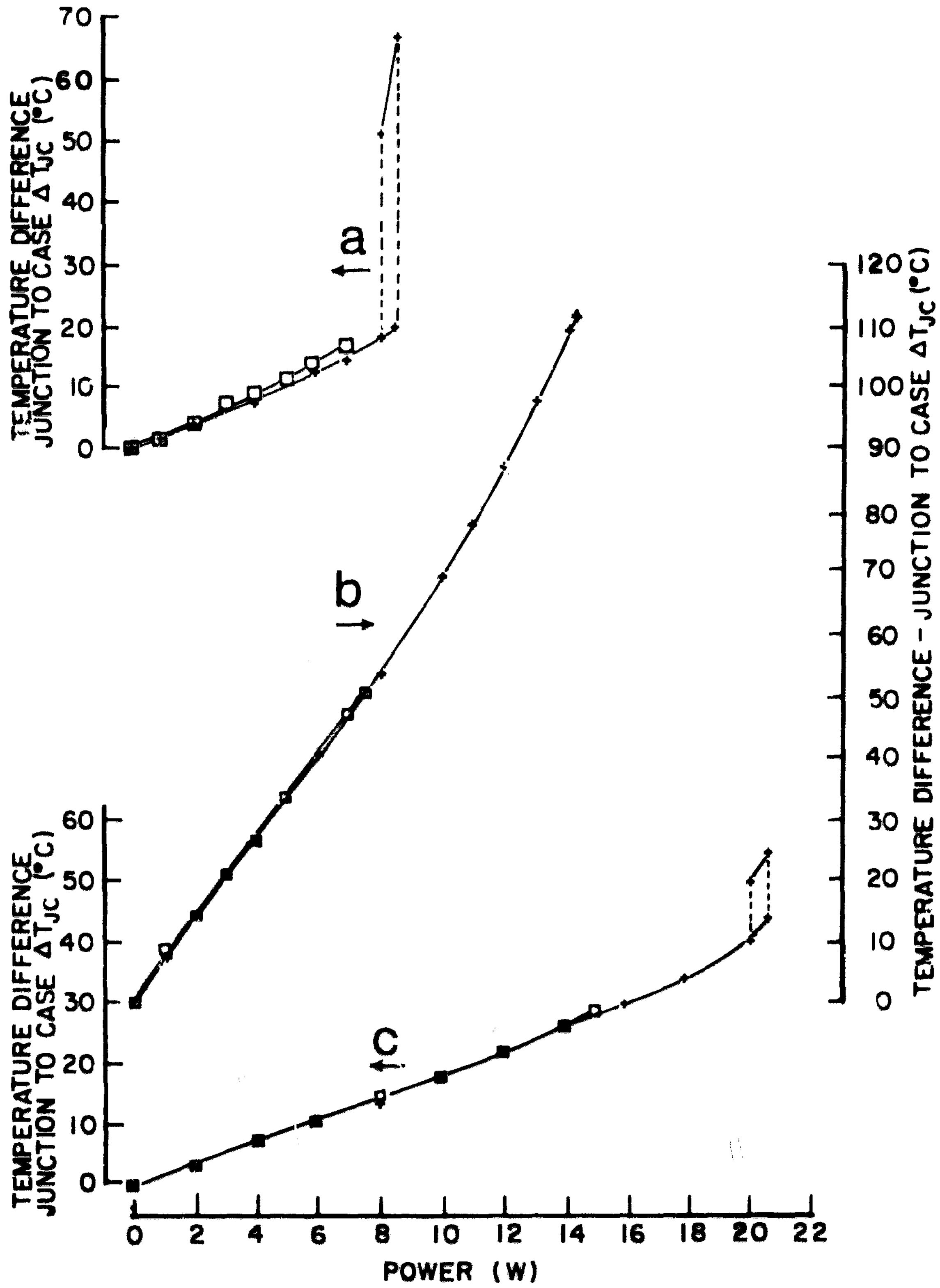

Fig. 17 Junction-to-case temperature difference as derived from measurements of base-emitter voltage as a function of applied power for three different device types. (Two collector current levels were used: 100 mA (□) and 200 mA (+). Case temperature was held at 25°C.)
a: 35-W, epitaxial-diffused, silicon power transistor.
b: 20-W, triple-diffused, silicon power transistor.
c: 35-W, triple-diffused, silicon power transistor.

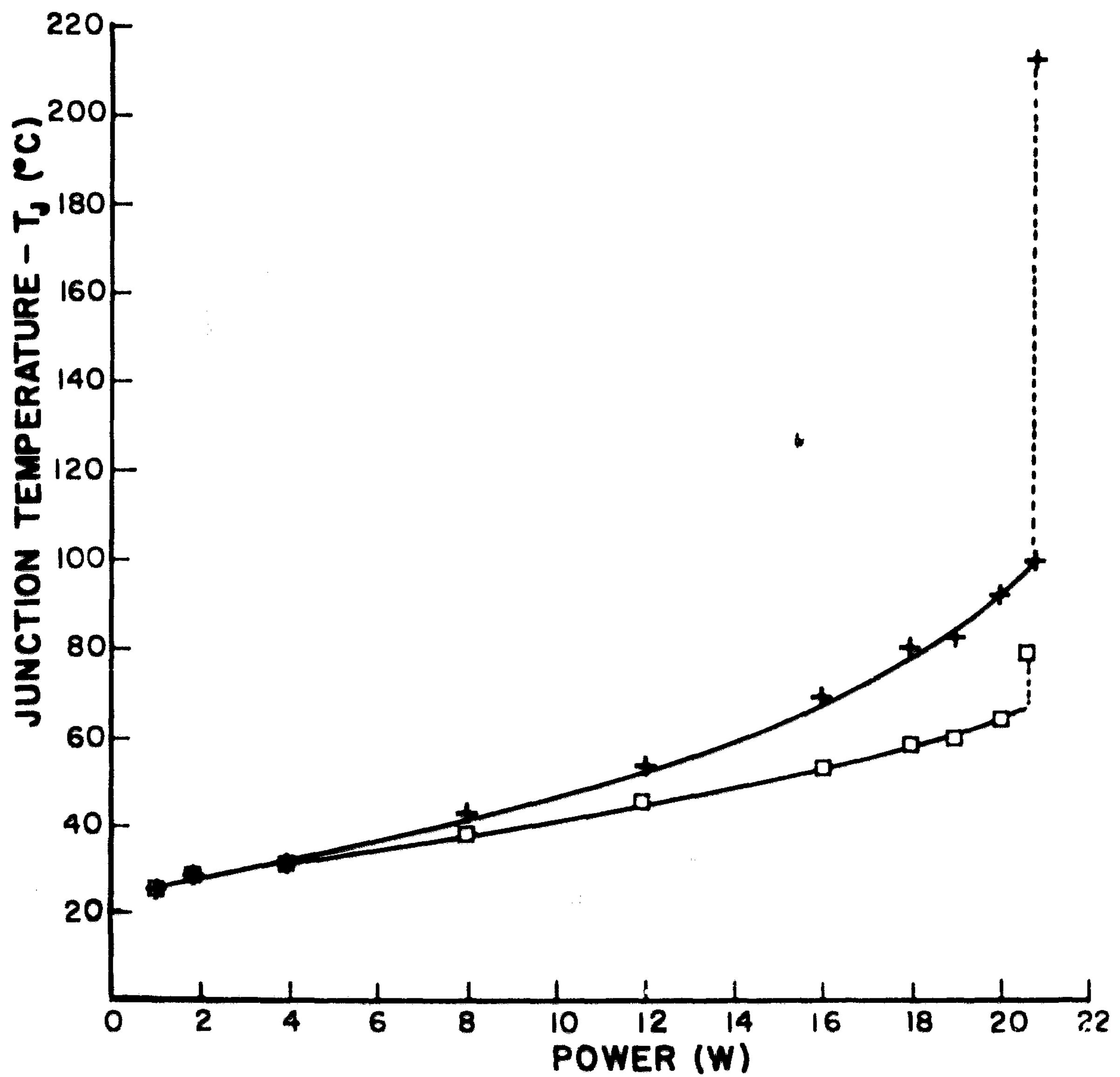

Fig. 18 Comparison of peak junction temperature with average junction temperature of a 35-W, triple-diffused, silicon power transistor. (Peak temperature measurements made with an infrared microradiometer (+) are significantly greater than average temperature derived from measurements of the base-emitter voltage (□) over much of the range. During application of power, collector current was 200 mA; case temperature was held at 25°C.)

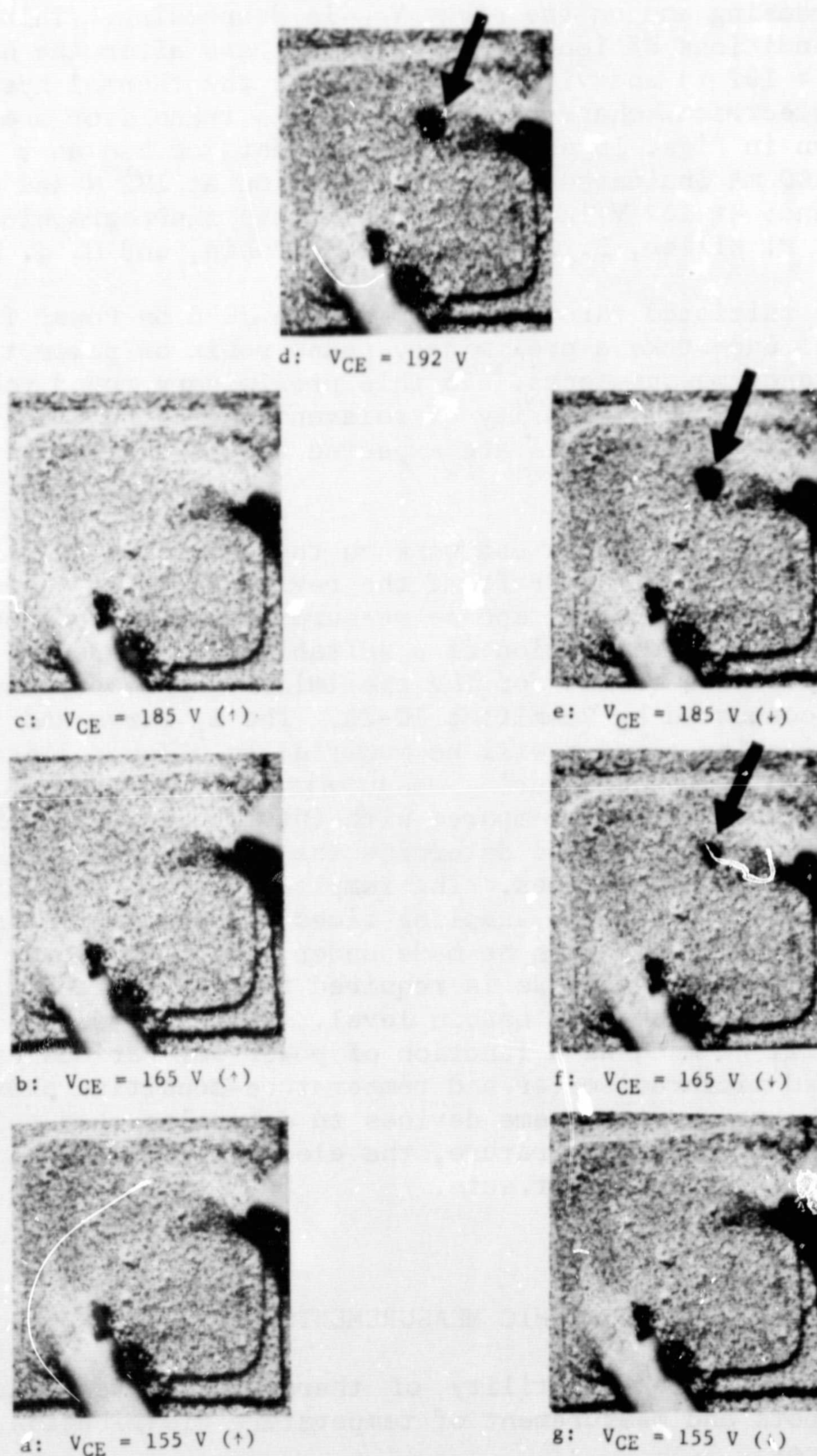

Fig. 19 Photomicrographs of a phosphor-coated, 35-W, triple-diffused, silicon power transistor under ultraviolet illumination. (Collector-emitter voltage was increased (a to d), then decreased (d to g). Collector current was held constant at 100 mA. The hot-spot is indicated by the arrow in d, e, and f. In d, the hot-spot temperature exceeds 250°C; in e and f, the hot-spot temperature exceeds 200°C.)

figure V_{CE} is increasing and on the right V_{CE} is decreasing. This arrangement pairs conditions of identical V_{CE} before and after the hot-spot is formed (at V_{CE} = 192 V) and vividly illustrates the thermal hysteresis phonomenon. The electrical characteristics of this transistor are similar to those shown in Figs. 16 and 18. Measurements of h_{FE} as a function of V_{CE} with I_B = 100 mA indicated hot-spot formation at 192 V and subsequent disappearance at 162 V in agreement with the thermographic study. (J. P. Miller, L. R. Williams, S. Rubin, and G. J. Rogers)

Work was also initiated through EIA Committee JS-6 on Power Transistors (now JC-25) to undertake a preliminary round robin on power transistor thermal resistance measurements. In this preliminary round robin emphasis is being placed on similarity of relevant operating conditions during measurement but participants are expected to use their existing R_Θ measuring equipment. (F. F. Oettinger)

Plans: The literature search and work on the bibliography will continue. The writing of the first draft of the review paper on thermal resistance and transient thermal response measurements will continue. Work will continue on the preparation of a suitable R_Θ measurement procedure and data collection format for the preliminary R_Θ measurement round robin being conducted by Committee JC-25. The I_B servo and the associated base switching circuit will be modified to allow collector currents of at least 1 A to be used during measurements of R_Θ and h_{FE}. Thermal inertia measurements will be compared with infrared microradiometer measurements in a further effort to determine the usefulness of electrically measured hot-spot temperatures. The sample-and-hold delay circuit will be modified to allow variable sampling times for the sample-and-hold system so that V_{BE} measurements can be made under higher collector current conditions where more than 6 µs is required for the switching transient in the base to decrease to a usable level. Thermal resistance and h_{FE} measurements will be made as a function of power for various ranges of V_{CE}, and infrared microradiometer and temperature-sensitive phosphor measurements will be made on the same devices to determine what relationships exist between the peak temperature, the electrically measured temperature, and thermal hysteresis effects.

5.2 THERMOGRAPHIC MEASUREMENTS

Objective: To evaluate the utility of thermographic techniques for detection of hot spots and measurement of temperature distribution in semiconductor devices.

Progress: Use of miniature, variable-intensity bulbs for ultraviolet illumination has improved the ease and accuracy of setting illumination levels. A photodiode is used as the ultraviolet light intensity monitor.

THERMOGRAPHIC MEASUREMENTS

The uniformity of the phosphor coating obtained by the flotation technique (NBS Tech. Note 488, p. 31) was checked by scanning twelve wafer segments obtained from seven different coating batches with the photometric microscope. Light output was uniform within about 10 percent for all samples. It was also found that phosphor luminance stabilizes within about 15 s after the phosphor reaches a given temperature within the recommended operating range of the phosphor. Outside this range, the phosphor luminance may take as long as 20 min to stabilize. Since 25°C is outside the recommended operating range of most of the phosphors, this lag must be taken into consideration when comparing the phosphor output at room temperature before and after high-temperature measurements.

Spatial resolution was found to be limited by the 60-µm resolution of the fiber-optic probe of the photometric microscope. In measuring hot-spot temperatures with the microscope it was found that a 225-µm diameter hot spot encountered in one transistor could not be measured accurately because of the light picked up by the probe from the lower-temperature (and hence brighter) areas surrounding the hot spot. This "background bias" made the temperature of the hot spot appear lower than its true value. How much of the surrounding area contributes to this bias has not been determined, but the intensity of the light from this area was, in some areas, as high as half the intensity from the hot-spot.

To determine the effectiveness of reducing the probe diameter (a probe with 20-µm resolution can be obtained) the hot-spot and chip dimensions were increased by a factor of three (675-µm diameter hot-spot and 4-mm square chip) and measurements made with the present probe. The maximum background bias was reduced to one tenth the light given off by the hot spot itself. Reducing the numerical aperature of the microscope to simulate the reduced light input obtainable from the smaller probe indicated the light levels would still be measurable with existing apparatus. (G. J. Rogers, F. F. Oettinger, J. P. Miller, and L. R. Williams)

Plans: Temperature calibration of the phosphors will be completed. Both the phosphors and the IR microscope will be used to examine the temperature distribution on the surface of power transistors. A smaller diameter probe will obtained for the photometric microscope.

5.3 MICROWAVE DEVICE MEASUREMENTS

Objective: To develop improved methods for the measurement of selected microwave device properties suitable for application in industrial and military specifications.

Progress: Design and construction of the i-f section of the X-band mixer measurement circuit has begun. Because it is difficult to make

precise immittance measurements at the normal i-f test frequency of 30 MHz, audio intermediate frequencies (generally 1-kHz square waves) are being used in performing the initial measurements. The greater precision possible at audio frequencies facilitates the study of mixer parameter dependence on i-f load and d-c bias. While theoretically independent of intermediate frequency, conversion loss measurements at audio and 30 MHz i-f's have generally not agreed in practice. Ascertaining the reasons for this is of great importance to the realization of accurate measurement standards because measurements at both frequencies have been widely used in the industry.

A circuit has been designed to measure instantaneous values of mixer output voltages at the millivolt level. It consists of a high-precision digital voltage source, an automatic switch, and an oscilloscope that has a d-c coupled, high-gain vertical amplifier with d-c offset control. The oscilloscope is switched periodically between the mixer output voltage and the reference voltage. The instantaneous value at any point on the mixer output audio i-f waveform may be determined by setting the reference voltage so that its trace intersects the i-f trace at that point.

A square wave has been introduced as the i-f signal. The oscilloscope comparison with a d-c voltage reference can be made more precisely and rapidly with a square wave than with a sine (or other) wave. Although conversion loss is most easily related to a sinusoidal (single-frequency) i-f signal, the accuracy of average-rectified or true-rms measurements using a sine wave is limited by modulator nonlinearity which makes a perfectly sinusoidal modulation impossible to obtain. When a square wave is used, the i-f output power calculations are made for a sine wave having the same peak-to-peak value. This assumes only that the circuit response is uniform over the range of significant harmonics. The rounding of corners due to high frequency attenuation can be ignored in making the oscilloscope measurement, so that it is sufficient to have a flat low and medium frequency response that provides a tilt-free waveform with no discernable ripple.

The use of a square-wave signal also facilitates the measurement of the available r-f signal power which is generated by amplitude modulation of the local oscillator. The peak-to-trough power ratio, from which the equivalent single-sideband r-f signal power is calculated, is easiest to measure using square-wave modulation: A precision attenuator in cascade with the modulator is used as a comparison standard; it is varied to produce the same change in output level as the modulator. The signal is observed with the d-c coupled oscilloscope periodically switched between the mixer and the reference supply as described above. The reference supply is, in this case, used only to provide an adjustable, stable, and parallax-free oscilloscope reference line, whose position relative to the mixer output waveform is independent of oscilloscope gain or position.

As with i-f output, the calculation of r-f signal power is for sinusoidal modulation with the same peak-to-trough ratio as that of the square-wave actually used. (J. M. Kenney)

A review of the state of accuracy in equipment for measurement of scattering-parameters of transistors was prepared for the Task Group on S-Parameter Measurement Standard of JEDEC Committee JS-9 on Low Power Transistors (now JC-24 on Signal Transistors). This review considered the three basic types of instruments that are used for transistor measurements above 100 MHz; the sensitivity and range of measurement of reflection coefficient, attenuation or gain, and related phase angles; anticipated errors; and the effect of test power level on errors. The review was presented at the August 12 meeting of the task group. (R. C. Powell)

Plans: Design and construction of the audio i-f section will continue. A circuit for measuring mixer i-f conductance at audio frequencies will be incorporated into the system. The audio i-f circuitry for measuring conversion loss will be retained for comparison with measurements made at 30 MHz.

5.4 CARRIER TRANSPORT IN JUNCTION DEVICES

Objective: To improve methods of measurement for charge carrier transport and related properties of junction semiconductor devices.

Background: A technical and economic need of high priority has developed in the application of semiconductor devices in government programs and in the development and evaluation of these devices by industry, specifically for use in a radiation environment. Prediction of transistor degradation in such an environment is frequently based on measurements of charge carrier transit time in the base region of the device (t_B), or on measurements of the frequency at which common-emitter current gain decreases to unity (f_T). Experience has shown that, at present, correlation between device degradation and values of t_B or f_T is inadequate, and further that measurements of these parameters cannot be adequately correlated with each other, even before exposure to radiation, when they are made on the same devices by use of different instruments in the same laboratory or in different laboratories on the same type of equipment. It is important that suitable techniques for measuring these characteristics be defined, and that new techniques be developed where necessary, in order to facilitate the design and evaluation of devices for government programs and for industry. Such improvements in measurement techniques are expected to permit a closer relationship to be made between the results of measurements made on the device and the physical processes occurring within the semiconductor material. In this way, one

will be better prepared to design or screen devices intended for operation in hostile (e.g., radiation) environments.

A further need is to develop the capability of measuring t_B and f_T for transistors in integrated circuits directly on the silicon wafer before the final packaging, that is the most costly step in production of these devices. Such measurements may be expected to be of value to process control and improvement for advanced devices for a variety of applications other than those involving radiation environments.

Progress: A preliminary survey of this problem for planning purposes was undertaken after the significance of the situation was called to the attention of the Division by an Air Force laboratory. Visits were made to a number of government and industrial organizations including the Air Force Weapons Laboratory, Rome Air Development Center, Space and Missiles Systems Organization, Air Force Materials Laboratory, Aerospace Corporation, Sandia Laboratories, and Strategic Project Office. The consensus of all the organizations visited was that the resolution of this problem by NBS is a matter of great importance both to solve the technical problem to the satisfaction of the variety of interests involved and to reduce the great expense involved in radiation exposure tests being conducted with inadequate measurement methods.

Laboratory work in the transit-time area began near the end of the quarter with the construction of a delay-time bridge and the specification and purchase of components for a system based on the use of a vector voltmeter. In addition, various methods in current use for the measurement of base-transit time and techniques intended to characterize devices in the wafer stage are being evaluated. (D. E. Sawyer)

Plans: Work will continue on review and evaluation of pertinent material from literature sources. Other laboratories will be visited to determine further the current state of the art in various transit-time measurement techniques. Work on the construction of the delay-time bridge will continue. The vector-voltmeter system will be assembled after the various components are delivered.

5.5 SILICON NUCLEAR RADIATION DETECTORS

Objective: To conduct a program of research, development, and device evaluation in the field of silicon nuclear radiation detectors with emphasis on the improvement of detector technology, and to provide consultation and specialized device fabrication services to the sponsor.

Progress: Two surface-barrier and five lithium-drifted silicon radiation detectors were given extensive pre-flight tests for the sponsor.

These included measurement of front and rear alpha-particle and beta-particle resolution at -10, 23, and 40°C, noise, capacitance-voltage, and current-voltage characteristics. One of the five Si(Li) detectors exhibited breakdown at 40°C and did not return to its previous characteristics when cooled to room temperature, indicating that the effects of temperature cycling are not always reversible. (J. M. Morrison)

The mechanical modification of the ultra-high vacuum system to accomodate up to 21 detectors for long-term study under space-simulated conditions was completed during the previous quarter. Electrical connections were installed during the current period. Plans call for this system to be attached to an external commercial refrigeration unit to permit cycling of the detectors from -20 to +40°C. Pending arrival of the refrigeration unit, three surface barrier detectors and three Si(Li) detectors, which had been fully bench tested, were installed into an adjacent temporary chamber to begin tests to determine their long-term performance. Data are now being collected on these detectors at room temperature and low pressure (near 10^{-6} torr). (Y. M. Liu)

Hydrazine thrusters on the forthcoming Pioneer F un-manned mission to Jupiter are expected to leave a thin shroud of ammonia and hydrazine around the spacecraft. In an effort to study the effects of such an ambient on the counting performance of silicon radiation detectors, an all-glass vacuum chamber and pumping system was assembled to provide a means for back-filling the test chamber containing a detector to a specified pressure with an ammonia mixture. (B. H. Audet and E. I. Klein)

The study of the electron damage effects in silicon surface barrier detectors has been completed [1]. In preparation for the next phase of the radiation damage study, fabrication of several lithium drifted silicon radiation detectors has begun. This work has so far been hampered by both surface and material problems. (Y. M. Liu and B. H. Audet)

Plans: Extensive pre-flight testing of silicon particle detectors will continue as required by the sponsor. Upon receipt and acceptance of the refrigeration unit, the ultra-high vacuum system will be completed, and long-term temperature cycling effects will be studied. The fabrication of Si(Li) detectors will continue and study of damage due to electron irradiation in these detectors will begin.

5.6 REFERENCES

5.5 Silicon Nuclear Radiation Detectors

1. Y. M. Liu and J. A. Coleman, "Electron Radiation Damage Effects in Silicon Surface Barrier Detectors", to be published in *IEEE Trans. Nucl. Sci.*

Appendix A

JOINT PROGRAM STAFF

Coordinator: J. C. French
Consultant: C. P. Marsden

Semiconductor Characterization Section
(301) 921-3625

Dr. W. M. Bullis, Chief

A. J. Baroody, Jr.
D. L. Blackburn
F. H. Brewer
Mrs. E. C. Cohen*
M. Cosman
Dr. J. R. Ehrstein
G. G. Harman
Mrs. R. E. Joel+
F. R. Kelly†
H. K. Kessler
Mrs. K. O. Leedy
Miss C. A. Main
R. L. Mattis
Dr. W. E. Phillips
Miss T. A. Poole+
Miss D. R. Ricks
H. A. Schafft
J. P. Sinkovic†
A. W. Stallings
G. N. Stenbakken
W. R. Thurber

Semiconductor Processing Section
(301) 921-3541

Dr. A. H. Sher, Acting Chief×

Miss D. A. Adamson†
B. H. Audet
Miss J. B. Boger†
H. A. Briscoe
W. K. Croll
Mrs. S. A. Davis+
H. E. Dyson*
J. A. Heath†
W. J. Keery
E. I. Klein
J. Krawczyk
T. F. Leedy
Y. M. Liu
Miss J. M. Morrison
J. Oroshnik
R. C. Schaevitz*†
Mrs. E. A. Simmons†
L. M. Smith
G. P. Spurlock

Electron Devices Section
(301) 921-3622

J. C. French, Chief

A. L. Baskin†
Mrs. C. F. Bolton+
Mrs. R. Y. Cowan
Miss B. S. Hope+
R. L. Gladhill
J. M. Kenney
J. P. Miller†
F. F. Oettinger
M. K. Phillips
R. C. Powell*
G. J. Rogers
S. Rubin
D. E. Sawyer
M. Sigman
L. R. Williams

---

* Part Time
\+ Secretary
† Summer
× Dr. J. A. Coleman is on temporary assignment to Office of Associate Director for Programs.

Appendix B

COMMITTEE ACTIVITIES

ASTM Committee F-1; Materials for Electron Devices and Microelectronics

- A. J. Baroody, Lifetime Section
- C. F. Bolton, Committee Assistant Secretary
- W. M. Bullis, Editor, Subcommittee 4, Semiconductor Crystals; Leaks, Resistivity, Mobility, Dielectrics, and Compound Semiconductors Sections
- J. A. Coleman, Secretary, Subcommittee 5, Semiconductor Processing Materials
- J. R. Ehrstein, Resistivity, Epitaxial Resistivity, and Epitaxial Thickness Sections
- J. C. French, Committee Editor
- T. F. Leedy, Photoresist Section
- C. P. Marsden, Committee Secretary
- R. L. Mattis, Lifetime Section
- J. Oroshnik, Thick Films and Photomasking Sections; Chairman, Thin Films Section
- W. E. Phillips, Crystal Perfection, Encapsulation, Thin Films, and Thick Films Sections; Chairman, Lifetime Section
- A. H. Sher, Germanium Section
- M. Sigman, Editor, Subcommittee 5, Semiconductor Processing Materials
- W. R. Thurber, Mobility, Germanium, and Impurities in Semiconductors Sections

Electronic Industries Association:

- F. F. Oettinger, Associate Member, MED 32, Active Digital Circuits; Task Group 41.6, Thermal Considerations, MED 41, Physical Characterization Requirements

Joint Electron Device Engineering Council (EIA-NEMA):

- J. M. Kenney, Microwave Diode Measurements, JS-3, UHF and Microwave Diodes
- F. F. Oettinger, Thermal Resistance Measurements, JS-1, Rectifier Diodes; Technical Advisor, JS-14, Thyristors; JS-2, Signal Diodes; JS-9, Low Power Transistors
- R. C. Powell, Microwave Diode Measurement, JS-3, UHF and Microwave Diodes; Task Group on Transistor Scattering Parameter Measurement Standards, JS-9, Low Power Transistors
- S. Rubin, Chairman, Council Task Group on Galvanomagnetic Devices
- H. A. Schafft, Consultant on Second Breakdown Specification, JS-6, Power Transistors

IEEE Electron Devices Group:

- J. C. French, Standards Committee
- J. M. Kenney, Chairman, Standards Committee Task Group on Microwave Solid State Devices II (Mixer and Video Detector Diodes)

APPENDIX B

IEEE Nuclear Science Group:

J. A. Coleman; Administrative Committee; Nuclear Instruments and Detectors Committee; Editorial Board, *Transactions on Nuclear Science;* Chairman, 1970 Nuclear Science Symposium

A. H. Sher, Technical Program Committee, 1970 Nuclear Science Symposium

IEEE Magnetics Group

S. Rubin, Chairman, Galvanomagnetic Standards Subcommittee

IEC TC47, Semiconductor Devices and Integrated Circuits:

F. F. Oettinger, U. S. Experts Advisory Committee

S. Rubin, Technical Expert, Galvanomagnetic Devices; U. S. Specialist for Working Group 5 on Hall Devices and Magnetoresistive Devices

NMAB Ad Hoc Committee on Electronic Materials and Devices:

W. M. Bullis

Appendix C

SOLID-STATE TECHNOLOGY & FABRICATION SERVICES

Technical services in areas of competence are provided to other NBS activities and other government agencies as they are requested. Usually these are short-term, specialized services that cannot be obtained through normal commercial channels. Such services provided during the last quarter are listed below and indicate the kinds of technology available to the program.

1. Sectioning and plating — (H. A. Briscoe)
   Transistors were sectioned, polished, and stained to reveal cross-sectional geometries and small piece parts were gold and indium plated for other groups in the Electronic Technology Division.

2. Quartz and glass fabrication — (E. I. Klein)
   a. A McLeod gage which will be used as a reference standard was fabricated for the Vacuum Measurements Section.
   b. Three quartz methane cells with optical windows were fabricated for the Quantum Electronics Section.
   c. A ground-glass-to-metal assembly was fabricated for the Vacuum Measurements Section.

Appendix D

JOINT PROGRAM PUBLICATIONS

Prior Reports:

A review of the early work leading to this Program is given in W. M. Bullis, "Measurement Methods for the Semiconductor Device Industry—A Review of NBS Activity," NBS Tech. Note 511, December, 1969.

Quarterly reports covering the period since July 1, 1968, have been issued under the title "Methods of Measurement for Semiconductor Materials, Process Control, and Devices."

Quarter Ending	NBS Tech. Note	Date Issued	DDC Accession No.
September 30, 1968	472	December, 1968	AD 681330
December 31, 1968	475	February, 1969	AD 683808
March 31, 1969	488	July, 1969	AD 692232
June 30, 1969	495	September, 1969	AD 695820
September 30, 1969	520	March, 1970	AD 702833
December 31, 1969	527	May, 1970	AD 710906
March 31, 1970	555	September, 1970	
June 30, 1970	560	November, 1970	

Current Publications:

A. H. Sher, "Nomographs for Use in the Fabrication and Testing of Ge(Li) Detectors," NBS Tech. Note 537, August, 1970.

W. M. Bullis, "Measurement Methods for Microcircuits," presented at ASTM/IES/AIEE Space Simulation Conference, Gaithersburg, September 14-16, 1970; *Space Simulation*, J. C. Richmond, Ed., NBS Spec. Publ. 336, October, 1970, pp. 449-455.

A. H. Sher, "Carrier Trapping in Ge(Li) Detectors," accepted for presentation at the 1970 Nuclear Science Symposium, New York, November, 1970.

Y. M. Liu and J. A. Coleman, "Electron Radiation Damage Effects in Silicon Surface-Barrier Detectors," accepted for presentation at the 1970 Nuclear Science Symposium, New York, November, 1970.

S. Rubin and F. F. Oettinger, "Thermal Hysteresis and its Possible Effect on Restriction of the Hot-Spot Free Operating Range of Some Power Transistors," to be published in *IEEE Trans. Electron Devices*.

FORM NBS-114A (1-71)

U.S. DEPT. OF COMM. BIBLIOGRAPHIC DATA SHEET	1. PUBLICATION OR REPORT NO. NBS TN 571	2. Gov't Accession No.	3. Recipient's Accession No.
4. TITLE AND SUBTITLE Methods of Measurement for Semiconductor Materials, Process Control, and Devices. Quarterly Report, July 1 to September 30, 1970			5. Publication Date April 1971
			6. Performing Organization Code
7. AUTHOR(S) W. Murray Bullis, Editor			8. Performing Organization
9. PERFORMING ORGANIZATION NAME AND ADDRESS NATIONAL BUREAU OF STANDARDS DEPARTMENT OF COMMERCE WASHINGTON, D.C. 20234			10. Project/Task/Work Unit No. See Item 15
			11. Contract/Grant No. See Item 12
12. Sponsoring Organization Name and Address Natl. Bureau of Standards, DASA (EA071-801), Navy Strategic Systems Project Office, NAD, Crane, Indiana (PO-1-0030 and PO-1-0041), Navy Electronics System Command (PO-1-1057), AEC, and NASA (S-70003-G)			13. Type of Report & Period Covered Interim July 1 to Sept. 30, 1970
			14. Sponsoring Agency Code

15. SUPPLEMENTARY NOTES 4251120, 4251123, 4251126, 4252114, 4252119, 4252128, 4252534, 4254111, 4254112, 4254115, 4254429, 4259425, 4259522, 4259533.

16. ABSTRACT (A 200-word or less factual summary of most significant information. If document includes a significant bibliography or literature survey, mention it here.)

This quarterly progress report, ninth of a series, describes NBS activities directed toward the development of methods of measurement for semiconductor materials, process control, and devices. Work is continuing on measurement of resistivity, carrier lifetime, and electrical inhomogeneities in semiconductor crystals; specification of germanium for gamma-ray detectors; evaluation of wire bonds, metallization adhesion, and die attachment; measurement of thermal properties of semiconductor devices; and characterization of silicon nuclear radiation detectors. New effort is being started on the measurement of transit-time and related carrier transport properties in junction devices. Supplementary data concerning staff, standards committee activities, technical services, and publications are included as appendixes.

Key Words (cont.): of measurement; microelectronics; microwave devices; nuclear radiation detectors; probe techniques (a-c); resistivity; semiconductor devices; semiconductor materials; semiconductor process control; silicon; thermal resistance; thermographic measurements; ultrasonic bonder; wire bonds.

17. KEY WORDS (Alphabetical order, separated by semicolons) Alpha-particle detectors; aluminum wire; base transit time; carrier lifetime; die attachment; electrical properties; epitaxial silicon; gamma-ray detectors; germanium; gold-doped silicon; metallization; methods (cont.)

18. AVAILABILITY STATEMENT	19. SECURITY CLASS (THIS REPORT)	21. NO. OF PAGES
[XX] UNLIMITED.	UNCLASSIFIED	58
[ ] FOR OFFICIAL DISTRIBUTION. DO NOT RELEASE TO NTIS.	20. SECURITY CLASS (THIS PAGE) UNCLASSIFIED	22. Price 60 cents

☆ U. S. GOVERNMENT PRINTING OFFICE : 1971 431-997/269